PROSTATE CARCINOGENESIS: DEPICTING A PROPOSED PATHWAY FOR PROSTATE CANCER PRECURSOR LESION DEVELOPMENT USING 3D ANIMATION

by
William Guzman Jr.

A thesis submitted to Johns Hopkins University
in conformity with the requirements
for the degree of Master of Arts

Baltimore, Maryland
March, 2020

ABSTRACT

Prostate cancer is one of the most common malignant neoplasms among men in Western countries (De Marzo et al. 2017). In 2020, there will be an estimated 191,930 American men diagnosed with prostate cancer, an almost 10% increase from 2019 (Siegel et al. 2020). Visual resources for understanding of the pathogenesis of prostate cancer development, and specifically the development of prostate cancer precursor lesions, are limited. A visual void exists between prostate cancer Pathologists presenting histological findings and those with differing prostate cancer specialties. Furthermore, prostate cancer is typically studied using two-dimensional microscopy slides, and it is often difficult to explain new three-dimensional spatial hypotheses and findings to those outside of the pathology field.

Recent pathological evidence suggests a new role for prostate infections and inflammation in prostate cancer development. This novel hypothesis has the potential to challenge the dogma that high grade prostatic intraepithelial neoplasia (HGPIN) serves as the direct precursor to prostate cancer development. Rather, new molecular pathologic evidence indicates that an inflammation-associated lesion termed proliferative inflammatory atrophy (PIA) may directly transition to prostate cancer. 3D visualization of prostate cancer is novel and important in itself due to the multi-focal and atypical pattern of growth, and it is consequently challenging to communicate this new prostate cancer precursor lesion development model.

To address the lack of comprehensive histological research representation, a 3D mechanism of disease animation was constructed which portrays a new proposition for precursor lesion development using novel radical prostatectomy specimen data. The animation outlines and describes the harmful effects inflicted upon luminal epithelium caused by bacterial toxins, such as colibactin, as well as oxidants produced by immune cells induced by chronic inflammation. By improving visual understanding of histological data, this 3D animation provides a platform to further clarify the current knowledge of prostate cancer in the context of bacterial infections and chronic inflammation.

William Guzman Jr.

CHAIRPERSONS OF THE SUPERVISORY COMMITTEE

Karen Sfanos, M.S., Ph.D., Preceptor
Associate Professor of Pathology, Oncology, and Urology, Sidney Kimmel Comprehensive Cancer Research Center, Johns Hopkins University School of Medicine

Timothy Phelps, M.S., F.A.M.I., Department Advisor
Professor, Director of Production and Illustration Services, Department of Art as Applied to Medicine, Johns Hopkins University School of Medicine

David Rini, M.F.A, C.M.I., F.A.M.I., Technical Advisor
Professor, Graduate Program Director, Department of Art as Applied to Medicine, Johns Hopkins University School of Medicine

ACKNOWLEDGEMENTS

This project was made possible by the skilled and devoted people that supported me with their knowledge and guidance. I am grateful to have had this opportunity to work with them and collaborate with them. I extend endless gratitude to:

Tim Phelps, my advisor, Professor in the Department of Art as Applied to Medicine. Thank you for your endless insight, encouragement, valuable feedback, attentiveness, and humor. Through his keen eye and storytelling expertise, I learned how to better depict accurate scientific subject matter.

Karen Sfanos, my preceptor, Associate Professor of Pathology, Oncology, and Urology. Thank you for guiding me through the incredible pathological journey of this topic. Your passion and admiration for research has been inspirational in helping me represent my project in a coherent and educational manner. Thank you for continuously providing your time, resources, and helpful comments.

David Rini, my technical advisor, Professor and Graduate Program Director in the Department of Art as Applied to Medicine. Thank you for sharing your knowledge on 3D manipulation techniques and assisting with asset construction.

The Faculty and Staff of the Department of Art as Applied to Medicine: **Corinne Sandone, David Rini, Jennifer Fairman, Lydia Gregg, Juan Garcia, Jeff Day, Gary Lees, Ian Suk, Donald Bliss, Anne Altemus, Norman Barker, Fabian De Kok-Mercado, Graham Johnson, Sandra**

Gabelli, Sarah Poynton, Mike Linkinhoker, Veronica Falconieri, Carol Pfeffer, and **Dacia Balch**. Thank you for the never-ending reassurance and support that helped me strive to become a better communicator.

My talented classmates in the Class of 2020: **Noelle Burgess, Jamie Peterson, Kellyn Sanders, Morgan Summerlin, Helen Tang,** and **Jenny Wang**. Thank you for your inspiration, countless hours of laughter, collaboration, and everlasting friendship.

My family: **William Guzman Sr., Marina Guzman, Jhoseline Guzman,** and **Wilmer Guzman**. Thank you for always being there for me whenever I needed it. Your constant support, love, and optimism throughout my life have fueled me to accomplish anything I set my mind to.

TABLE OF CONTENTS

LIST OF FIGURES

INTRODUCTION

Overview of the Prostate

The word 'prostate' is derived from Greek word *prostates* which means "protector" or "someone who stands before someone or something," (Sfanos et al. 2017). The prostate is a small walnut-sized organ that sits between the bladder and the penis, along with the majority of the male reproductive system including the epididymis, testicles, and vas deferens (Sfanos et al. 2017). The average size of the prostate is 3.4 cm in length, 4.4 cm in width, and 2.6 cm in thickness, with a weight ranging from 15 to 20 grams (Amis, 1994). The orientation of the prostate is determined by the superior most portion, known as the base, and the inferior most portion, known as the apex. The adult prostate is traversed by paired ejaculatory ducts that enter the prostate superiorly where they join the prostatic urethra about midway to the center of the prostate (Amis, 1994).

The prostate is composed of five zones that use the prostatic urethra as the reference point: the central zone, anterior fibromuscular zone, transition zone, peripheral zone, and periurethral zone. The central zone encompasses the posterior superior region of the prostate that surrounds the ejaculatory ducts (Aaron et al. 2017). The central zone composes roughly 25% of the glandular prostate and branches laterally near the prostatic base (McNeal, 1981). The lateral borders of the central zone fuses with the proximal peripheral zone border to continue its region with the peripheral zone (McNeal, 1981). The anterior fibromuscular zone covers the anterior surface of the prostate, protecting the prostate with thick connective tissue (McNeal, 1981). The anterior fibromuscular

zone extends from the base to the apex. The transition zone lies just posterior to the anterior fibromuscular zone and accounts for about 5% of total prostatic volume in a normal, non-diseased prostate (McNeal, 1981). The transition zone surrounds the anterior portion of the prostatic urethra and is the main site for the location of benign prostatic hyperplasia (BPH) pathogenesis (Aaron et al. 2017). The peripheral zone surrounds the entire posterolateral surface of the prostate and extends anteriorly until meeting with the anterior fibromuscular stroma (Amis, 1994). Constituting more than 70% of glandular tissue in the prostate, the peripheral zone surrounds the posterior region of the central zone, spanning from the base to the apex of the prostate (McNeal, 1981). The majority of prostate cancer (75-80%) occurs in the peripheral zone and the remaining cancers arise from the transition zone and, rarely, the central zone (McNeal et al. 1988). The periurethral zone is the region within the prostate that wraps around the entirety of the prostatic urethra, spanning from the superior portion of the prostatic urethra to the inferior portion.

Histology of the Prostate

The zones of the prostate are composed of stroma, or fibromuscular tissue containing ductal networks. Ductal networks within the stroma are known as glands. Prostatic glands are composed of pseudostratified luminal epithelial cells that have direct contact with the lumen of the gland (**Figure 1**). Supporting the luminal epithelium are basal cells. Basal epithelium has direct contact with the stroma and is not present in the lumen of the gland. Both luminal and/or basal cell types provide implications for tumor stratification and have been intensively studied for prostate cancer origin (Wang et al. 2015).

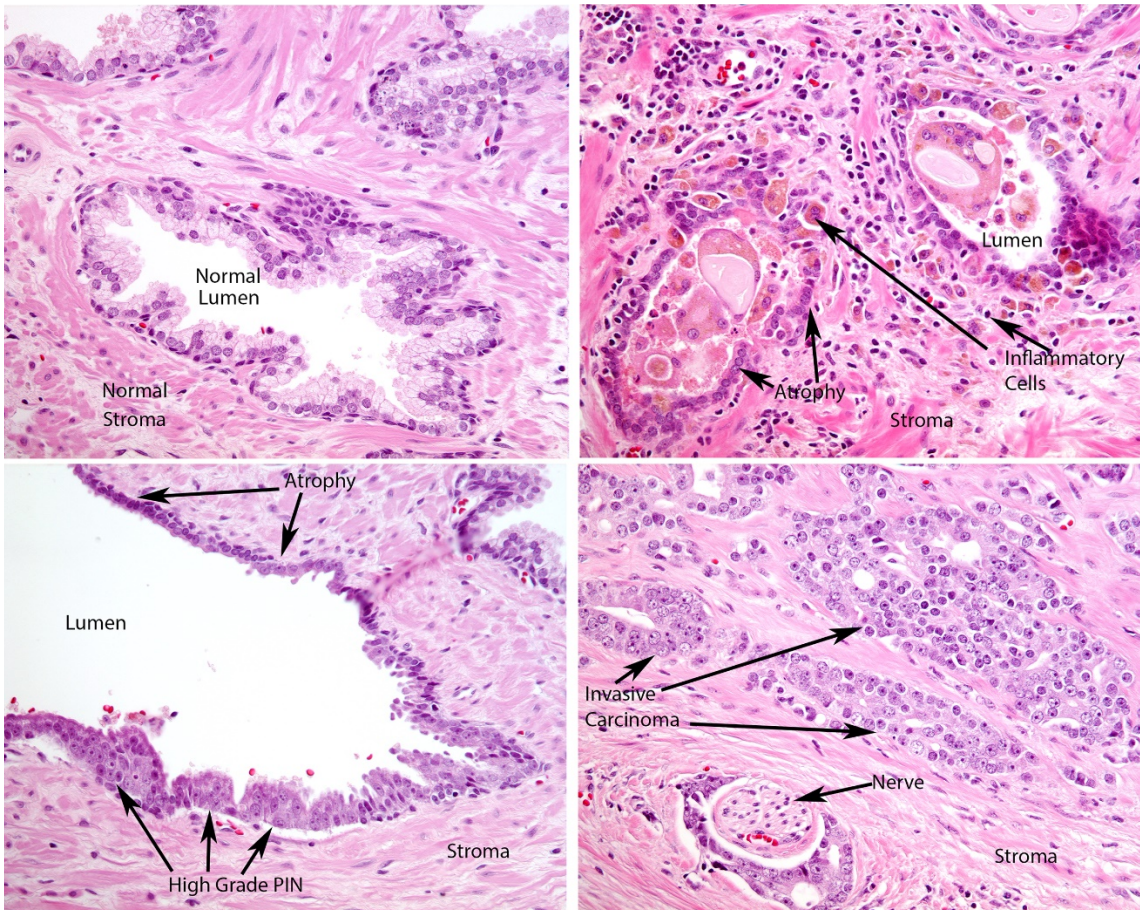

Figure 1. Luminal Epithelium Histology. These microscope slide images display the histology of the prostate (De Marzo et al. 2007).

Luminal cells line the epithelium and express androgen receptors (AR) and produce secretory proteins such as prostate-specific antigens (PSA) and prostatic acid phosphatase (PAP) (Zhang et al. 2019). There is strong evidence that luminal cells are the cell of origin for prostate tumors, including shared genetic and epigenetic alterations such as *GSTP1* methylation, telomere shortening, and MYC overexpression, in luminal cells in the presumed prostate cancer precursor lesion prostatic intraepithelial neoplasia (PIN) and cancer cells (Strand et al. 2015; Trabzonlu et al. 2018). When luminal cells reproduce, they are highly plastic in their differentiation capability (Horton et al. 2019).

Basal cells create the basement structure of the prostatic gland, composing a thin sheet of simple squamous cells forming a barrier between the luminal epithelium of the gland and the fibromuscular stroma. Proliferation of basal cells in the prostate varies from carcinoma to hyperplasia, but carcinoma arising from basal cells is exceedingly rare (Shibuya et al. 2018).

The stromal tissue of the prostate is composed of myofibroblasts, endothelial cells, fibroblasts, and immune cells (Krušlin et al. 2015). Collagens, elastic fibers, and laminins are also crucial components to stromal integrity. Collagens are fibrillar proteins that are important to cellular signaling processes and metabolism throughout the prostate (Krušlin et al. 2015). Elastic fibers aid in tissue flexibility and play a role in tumor invasion, but its exact role is not entirely understood (Krušlin et al. 2015). Laminins are molecules that reside primarily in basement membranes (Krušlin et al. 2015). Some research has shown a dramatic decrease in laminin expression in the stroma surrounding prostate carcinoma as compared to other regions of prostatic tissue (Tomas et al. 2006).

Corpora amylacea (CA) are a common occurrence within prostate glands and often seen when studying prostate cancer histology under the microscope. Corpora amylacea are small laminated bodies that can vary in size from a few millimeters to several centimeters in diameter (Sfanos et al. 2009). Prostatic calculi (PC), or calcified stones, can also be observed within the lumen and are related to corpora amylacea (Sfanos et al. 2009). The presence of CA/PC have been observed in prostate specimens with focal acute and chronic inflammation, gland occlusions, and epithelial trauma, and are thought to form during acute inflammatory events following prostate infection (Sfanos et al. 2009).

Prostate Cancer

Prostate cancer is one of the most common malignant neoplasms among men in Western countries (De Marzo et al. 2007). Prostate cancer is most common among men over the age of 65 and is prevalent in men of African descent (Kooh et al. 2019). Prostatic adenocarcinoma is primarily composed of malignancy in the epithelial cells and invasion of the surrounding stroma (Krušlin et al. 2015). Recently, a new hypothesis for prostate cancer precursor lesion development has been proposed, with a primary focus on the effects of the microenvironment and associated chronic inflammation within the prostate (De Marzo et al. 2007).

Chronic and recurrent inflammation have been linked to the pathogenesis of prostate cancer development (Nelson et al. 2012). The human urinary microbiome, and specifically urinary pathogens that can initiate prostate infections, have been proposed to influence the development of prostate cancer precursor lesions through direct and indirect interactions (Porter et al. 2018). The exact causes of prostate cancer are not well understood, but substantial evidence from various areas of cancer study point to multiple factors including diet, smoking, obesity, and environmental exposures contributing to development.

Inflammation

Approximately 20% of human adult cancers are a result from chronic inflammation and/or chronic inflammatory states (De Marzo et al. 2007). Not only is inflammation observed in prostate cancers, but it is observed in other

cancers associated with: stomach, large intestine, lung, pancreas, and esophageal cancers (De Marzo et al. 2007). The occurrence of prostatic inflammation within the male population is also associated with race and the geographical location of cancer patients (Sfanos et al. 2014). Biopsy specimens with chronic inflammation have shown to be more common in African American men than in European American men (Sfanos et al. 2014).

Inflammation within the prostate has been hypothesized to be a contributor to cancer development due to the frequent observation of inflammatory cells in the prostatic microenvironment of men (Sfanos et al. 2018). Chronic inflammation has been linked to the development of precursor lesions known as proliferative inflammatory atrophy (PIA) within the prostate (De Marzo et al. 2007). PIA lesions are classified as central areas of epithelial atrophy containing proliferative epithelial cells that are proposedly regenerative in nature (Nelson et al. 2003). The frequent findings of PIA lesions in prostate specimens exposed to chronic inflammation may be a consequence of inflammatory oxidants (Nelson et al. 2003). The contribution of inflammation can be seen in histological analysis of adult prostates removed for the treatment of both cancer and benign prostatic diseases (Sfanos et al. 2018).

The persistent presence of inflammatory cells in the prostate may produce large amounts of microbicidal oxidants (Nelson et al. 2003). Inflammatory cells are known to secrete cytokines which increase epithelial cell proliferation, increasing the risk of mutation. With chronic persistence of inflammatory cells within the prostate glands, mutations are more likely to occur as epithelial cells proliferate (De Marzo et al. 2007).

Microbiome

Recently, the urinary microbiome and prostate infections have been the prime subject of investigation in understanding the pathogenesis of prostate cancer precursor lesions (Shrestha et al. 2018; Peiffer et al. 2019). In the human body, microbes affect a large amount of pathophysiological processes (Kovacs et al. 2020; Manzoor et al. 2017). Any change in the quantity or composition of the microbiome can be associated with diseases (Kovacs et al. 2020). The urinary tract is an example of such interactions between the microbiota and the host (Manzoor et al. 2017).

Approximately 50% of men will have experienced some degree of prostatitis in their lifetime (Lupo et al. 2019). Bacteria colonize the prostate via ascension of the urethra to cause urinary tract infections (UTI) (Lupo et al. 2019). The prostate likely does not contain commensal microbial flora, but rather the prostate is populated by microorganisms in a pathological manner with focal regions associated with acute or chronic inflammation (Sfanos et al. 2017; Sfanos et al. 2008). Pathogenic organisms may also be contracted into the prostate via the urethra including sexually transmitted diseases, such as *gonorrhea*, *chlamydia*, *Trichomonas vaginalis*, and *Treponema pallidum* (De Marzo et al. 2007).

In a normal functioning prostate, the prostatic fluid contains elevated levels of antimicrobial components such as zinc, citrate, and antimicrobial peptides to prevent infection (Sfanos et al. 2017). Hypothetically, the healthy human prostate contains little to no organisms, which are not pro-inflammatory when the lumen epithelial layer is intact and with normal amounts of

antimicrobial secretions (Sfanos et al. 2017). As pathogenic bacteria migrate to the lumen of the prostate glands, a robust inflammatory response occurs, which is likely concurrent with the development of prostatic atrophy (Sfanos et al. 2017). The integrity of the luminal epithelial barrier may become disrupted as a result of inflammatory cell disruption of the cell layers, allowing bacteria to invade the stroma and surrounding tissues (Sfanos et al. 2017) (**Figure 2**). This results in further inflammatory response, perhaps resulting in a self-perpetuating inflammatory loop (Sfanos et al. 2017).

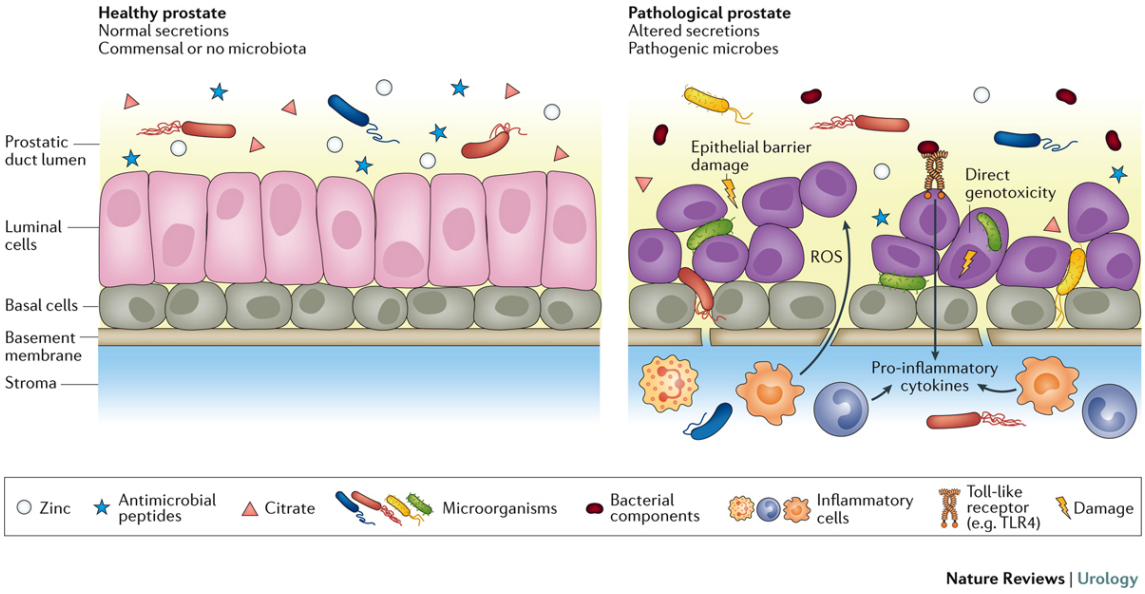

Figure 2. Prostatic inflammation induced by epithelial barrier breach. Depicted on the left image is a normal prostatic gland with proposed microorganisms in the prostatic secretions. As foreign bacteria enter the prostate via urinary reflux, toxins are produced which cause inflammation and distortion of the epithelial tissue. The right image shows the resulting disruption that may allow microorganisms to leave the lumen and enter the stroma to cause further inflammation (Sfanos et al. 2017). Text not inteded to be read.

Detection and Treatment

Prostate cancer is the most frequently diagnosed cancer in American men (Dhanasekaran et al. 2001). Although prostate cancer tends to be localized and unlikely to result in patient death, screening for prostate cancer is not well optimized to differentiate between indolent and aggressive carcinoma (Kooh et al. 2019). As prostate cancer progresses and metastasizes to distant tissues and structures, the likelihood of curing the cancer decreases (Leeuwen et al. 2019). This places the screening process as a pivotal determinant to confirm the presence/severity of cancer. Different methods to screen for prostate cancer are used, such as testing for elevated prostate specific antigen (PSA), digital rectal exam (DRE), and MRI imaging.

PSA screening is a blood-based biomarker that tests for enzymes produced almost exclusively by the prostate gland (Koo et al. 2019). Although screening for PSA allows for early detection, elevated PSA levels may also be present in non-malignant pathological conditions such as benign prostatic hyperplasia (BPH) as well as prostatic inflammation (Dhanasekaran et al. 2001). Lately, using PSA as a cancer screening biomarker has been known to provide false-negative and false-positive diagnoses (Koo et al. 2019). With the unreliability of PSA testing as a diagnostic tool, patients are placed at risk to be over-biopsied for cancer that they do not have or over-treated for a cancer that would never have killed them (Koo et al. 2019).

Patients with positive PSA screening tests will be referred for a surgical biopsy to further confirm cancer diagnosis. When performing a biopsy on the

prostate, the surgeon may use one of many procedures depending on the patient's condition and the healthcare provider's practices such as: the transrectal method, the perineal method, and the transurethral method (Johns Hopkins Medicine, 2020). The biopsy relies on removing prostate tissue samples from regions associated to the patient's proposed cancer location(s). "[While] the detection of prostate cancer in the biopsy ranges from 25% to 48%, this rate decreases between 10% and 25% in the case of repeat biopsy," (Karakiewicz et al. 2018).

MRI imaging is becoming a more commonly used tool in the cancer screening process. Typically, patients may receive MRI scans if the health provider decides to complete further conclusive tests after biopsy results (NIHR, 2017). Although MRI scans are a new valuable asset for prostate cancer detection, MRI findings may not always provide accurate results in patients with previous negative biopsies (Karakiewicz et al. 2018).

Radical prostatectomy, or complete surgical removal of the prostate, is a widely performed procedure to treat prostate cancer. Though radical prostatectomy is the most common procedure for men diagnosed with prostate cancer, surgery is associated with small long-term reductions in mortality and increases of life gained (Wilt et al. 2020). Radical prostatectomy can be used to cure locally confined prostate cancer, but the likelihood of curing the patient reduces with advanced metastatic cancer (Leeuwen et al. 2019; Toom et al. 2019).

Objectives

This project focused on the visualization of a new proposed pathway of development of prostate cancer precursor lesions through three main objectives:

1. **Create** 3D models and motion graphics using a third-party rendering engine.
2. **Design** a short animation that contextualizes recent evidence on prostate cancer precursor lesion development using computer graphics imaging and novel histological data.
3. **Communicate** the new proposed hypothesis to researchers that specialize in oncology.

Audience

The primary audience for this animation is cancer researchers that do not specialize in prostate cancer research. These individuals are well versed in cancer research, but have little exposure or knowledge of prostate cancer development. This project can also be used by a secondary audience of graduate students with an interest in learning more about prostate cancer pathways.

MATERIALS AND METHODS

Software Overview

A number of digital programs and software plugins were used to create storyboards, record audio, build 3D models, animate, and composite the renders. Adobe Photoshop CC 2020®, Adobe After Effects CC 2020®, Adobe Audition CC 2020®, Pixologic ZBrush®, Maxon Cinema 4D R20®, Redshift® for Cinema 4D.

Adobe Photoshop CC 2020 was used to create storyboards for the preliminary animation. Adobe After Effects CC 2020 was used for compositing images from Photoshop for the preliminary animation, known as the animatic, as well as the final compositing for the final renders created by the 3D software. Adobe Audition CC 2020 was used for recording and editing the audio for the animatic and final animation. Through Pixologic ZBrush, complex meshes and geometry were created that were otherwise difficult to create in Cinema 4D R20. Cinema 4D R20 was used to create 3D models, manipulate 3D models, and add motion graphics. Redshift for Cinema 4D, a third-party plugin, was used as the rendering engine to create quick preview renders, adjust lighting, materials, increase rendering efficiency, and used to generate the final renders.

Content Aggregation

Research from *The Sfanos Laboratory* was obtained in the form of publications and novel histological prostatectomy data. The first titled, 'The Inflammatory Microenvironment and Microbiome in Prostate Cancer Development' (Sfanos et al. 2017). The second publication titled 'Inflammation

in Prostate Carcinogenesis' (De Marzo et al. 2007). The third is titled 'Prostate Cancer' (Nelson et al. 2012). These publications provided a general overview of understanding the development of prostate cancer within the context of chronic inflammation and the microbiome. Along with these publications were histological slides depicting the progression and development of the risk factor lesions that are believed to be progenitors for prostate cancer. Additional information and data were gathered from related publications to the topic.

Script and Narration Development

For visualization of the prostate cancer precursor lesions, a script was developed to focus on the histological findings from *The Sfanos Laboratory*. The script covered the method in which pathologists commonly study the prostate, the techniques used to stain the prostate specimens, and the significance of these new findings. Careful wording was used to appropriately describe complex topics within the proposed pathway to better communicate this unfamiliar hypothesis to the intended audience. The script was narrated and the audio was recorded to then edit in Adobe Audition CC 2020.

Storyboard Development

A storyboard was created to act as the preliminary animation to the final 3D animation. In order to create the storyboard, Adobe Photoshop CC 2020 was used to draw 2D representations of scenes and models to create in the various 3D programs.

The storyboard was edited a total of three times prior to becoming finalized. Feedback from the Principal Investigator of *The Sfanos Laboratory* was used for revisions. After the 2D stills from Adobe Photoshop CC 2020 were approved, the animatic was created and the edited audio from Adobe Audition CC 2020 was inserted to adjust the timing between the words and the visuals.

3D Asset Creation

Creating a Prostate in Zbrush

The introduction to the animatic composed of a 3D representation of the adult prostate with its accompanying sectioning is similar to the method used by pathologists when studying prostatic tissue. Using measurements and photographic dissection references supplied by the Principal Investigator of *The Sfanos Laboratory*, the prostate was digitally sculpted with the 3D sculpting program Pixologic ZBrush. A Zbrush subtool in the form of a sphere was used as the preliminary shape for sculpting the prostate (**Tool** > **Sphere3D**). After selecting the sphere subtool, the sphere was dragged onto the canvas and the sculpting cursor was changed from **Draw** to **Edit**. Photographic references and measurements were then used to deform the sphere using the **Move Topological Brush** preset. Once the sphere mesh was deformed to an adequate shape of a normal adult prostate, the mesh needed to be re-topologized to account for the stretched polygons was caused by the **Move Topological Brush** (**Figure 3**). The mesh was re-topologized using ZRemesher and occasionally adjusted with the **Target Polygons Count** drag bar. This process was repeated

many times until an anatomically accurate model of the prostate body was developed.

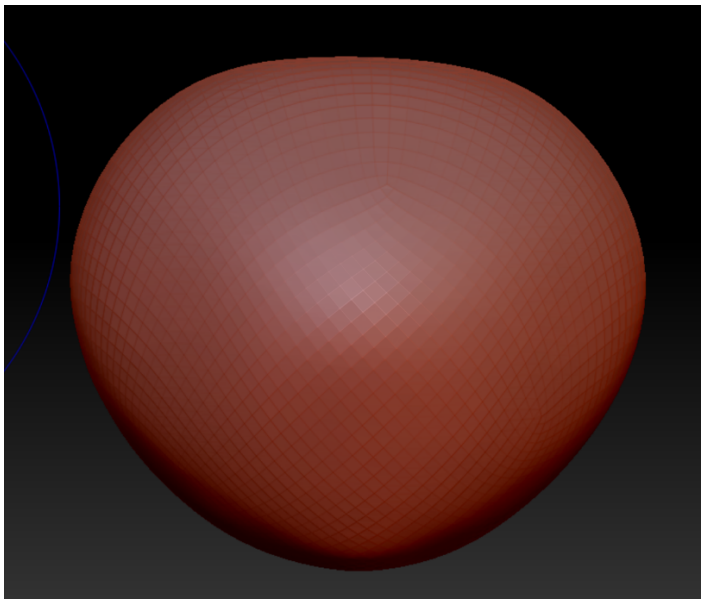

Figure 3. Anterior view of the prostate model. The prostate form is sculpted in ZBrush after using the Move Topological Brush.

Next, the prostatic urethra and the paired ejaculatory ducts that course through the prostate were sculpted. Histological cross sections were used as reference material for the approximate location of the prostatic urethra and ejaculatory ducts. In order to create these channels within the prostate, cylindrical meshes were imported onto the canvas and appended as new subtools. With the urethra subtool selected, the mesh was subdivided for clean manipulation of the topology without creating jagged edges (**Geometry** > **Subdivide**). The topology for the urethra was limited to a mesh consisting of less than five hundred thousand ActivePoints to reduce the complexity and memory size of the final prostate model for exporting/importing. The prostatic urethra

mesh was also well controlled using **ZRemesher** to retain clean and even topology after each drastic manipulation of the mesh. The shape for the prostatic urethra was manipulated by pushing and pulling the geometry using the **Standard Brush** and the **Move Topological Brush** from the **Brush Palette**. Once the adequate size, shape, and positioning of the urethra were achieved, the mesh was combined to the prostate and subtracted using **Live Boolean**. The urethra subtool was moved below the prostate subtool in the Subtool Palette and the appropriate Boolean Subtract icon was turned on to subtract the second subtool from the previous subtool in the Subtool Palette (**Boolean** > **Make Boolean Mesh**). Afterwards, a new tool was generated as the end product of the urethra subtraction from the prostate, leaving a channel within the prostate. The new combination of prostate and urethra was introduced to the subtool palette for the creation of the ejaculatory ducts (**Append** > **UMesh_Postate**).

To create the ejaculatory ducts, a cylinder was sculpted and manipulated in the same fashion as the prostatic urethra. After the ejaculatory duct for one side was finished, the subtool was duplicated and mirrored to create an exact copy of the subtool for the opposing duct (**Zplugin** > **SubTool Master** > **Mirror** > Select: **Merge into one SubTool** & **X axis**).

The prostate model, with the new prostatic urethra and two ejaculatory ducts, was then sculpted further to simulate the texture and form of an actual human prostate (**Figure 4**). Using the polygon subdivision command (**Ctrl** + **D**), the prostate mesh was taken to an ActivePoints count of less than one million polygons to reduce the exporting size of the mesh kept at a high ActivePoints count to retain fine sculpting details. The Standard Brush was used to digitally

sculpt the prostate model in combination with a custom Alpha channel by dragging a black and white polygon displacement map over large areas one at a time (**Alpha** > [Choose desired alpha channel]). This technique resulted in realistic prostatic tissue similar to prostatectomy specimens seen in the provided pathology photographs (**Figure 2**). After sufficient texturing was completed, the prostate model was exported as an OBJ file (**Export** [SubTool Palette] > **Save as format: OBJ**).

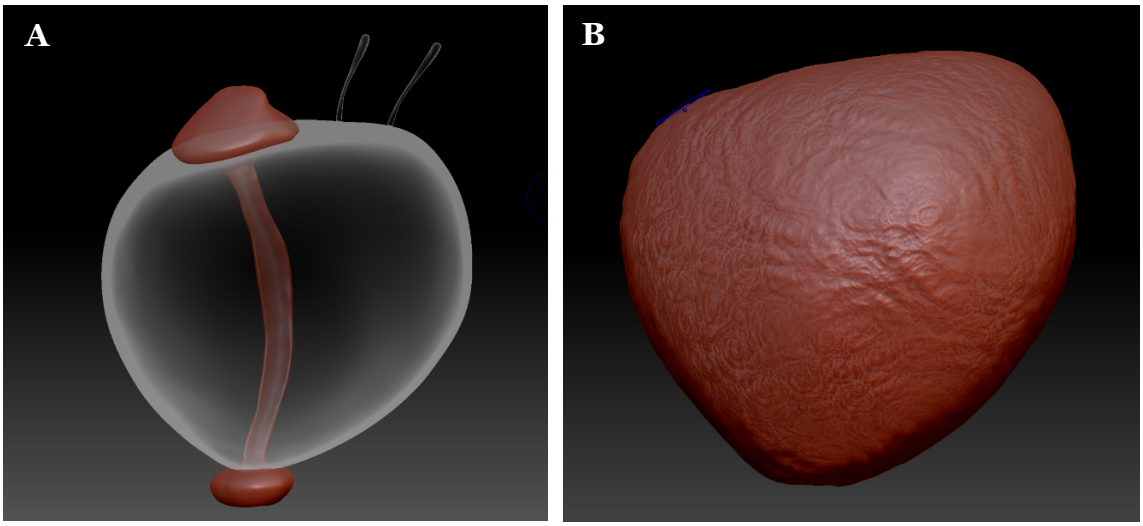

Figure 4. Boolean Subtraction and prostate texturing methods. The model is shown after meshes were created for subtraction as well as alpha brush sculpting. **(A)** Oblique anterior view of meshes for prostatic urethra and ejaculatory ducts. **(B)** Lateral view of prostate model with new surface texture.

The next scene in the animation displayed the prostate sliced, similar to the method used by pathologists to study the prostate under a microscope. To separate the prostate into multiple slices, Boolean subtraction was used in combination with re-topologizing techniques. Pathologists transversely dissect the prostate into six to ten slices depending on the size of the prostate. Eight rectangular prisms were appended to the Subtool Palette and were evenly spaced in the Y-axis of the model (**Append** > **PM3D_Cube3D**). Each rectangular prism was subdivided to ensure equal ActivePoints with the prostate mesh (**Ctrl** + **D**) and then subtracted from the previous rectangular prism to 'slice away' the previous mesh. Once the new combined Boolean mesh was created, the resulting subtool was saved as a new ZPR file and used for the next slice (**Figure 5**). This process was repeated seven more times to complete the remaining slices.

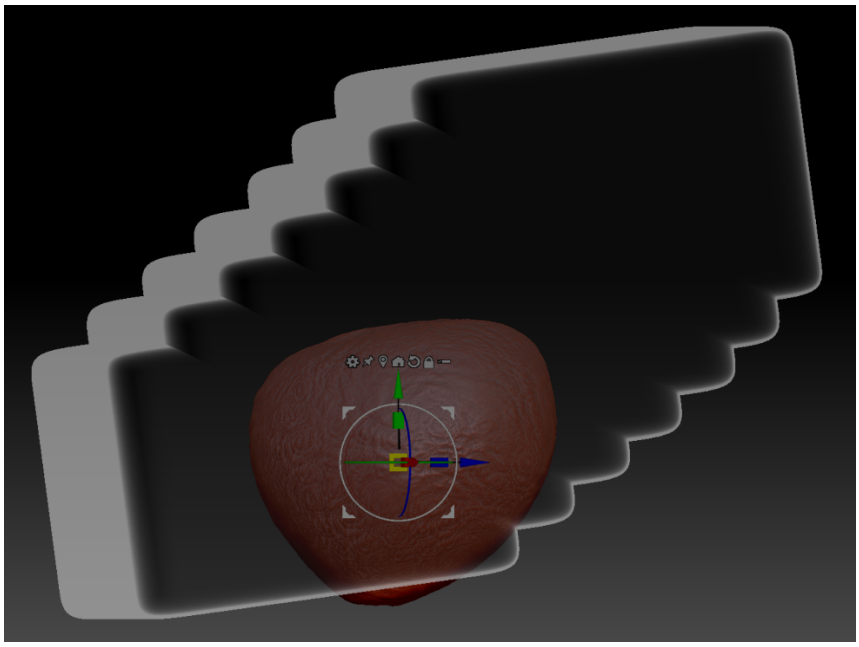

Figure 5. Sectioning the prostate model. The prostate model with the seven Boolean Subtraction rectangular prisms for slicing.

Once the desired slice thickness was achieved, each ZPR file was saved and sculpted separately to simulate the texture of stroma when the prostate is sliced open. Prior to texturing the stromal surface, the prostate slice was re-topologized to remove any broken geometry caused by the Boolean subtraction (**Geometry** > **ZRemesher** > **ZRemesher**). The new polygon count for each slice was kept under seven hundred thousand ActivePoints (**ZPlugin** > **Decimation Master** > **Pre-process Current** > **Decimate Current**). Boolean subtraction created more polygons to the prostate model and added fourteen new planar surfaces in between each slice, thus requiring additional polygon reductions to keep the size of the file as small as possible. It was crucial to not manipulate the coordinate location of the prostate slices as it would be very difficult to realign the slices to the correct X, Y and Z-axis from which they were Boolean subtracted. The eight slices were then separately exported as OBJ files to animate in C4D (**Export** [SubTool Palette] > **Save as format: OBJ**) (**Figure 6**). The slices were then imported into Cinema 4D for Redshift material application (**Figure 7**).

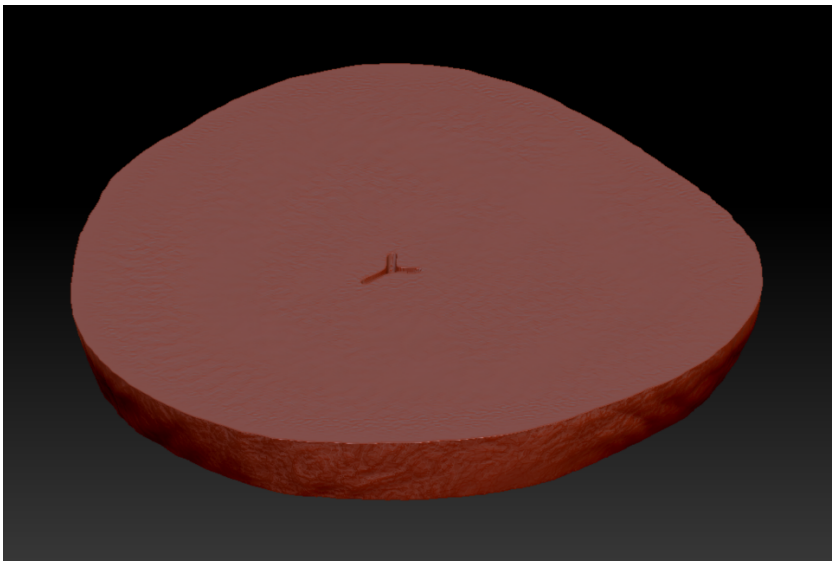

Figure 6. Resulting prostate slice from Boolean Subtraction. The model shown is of a slice of prostate after the completed Boolean Subtraction method along with stromal texturing created with the use of an alpha channel brush.

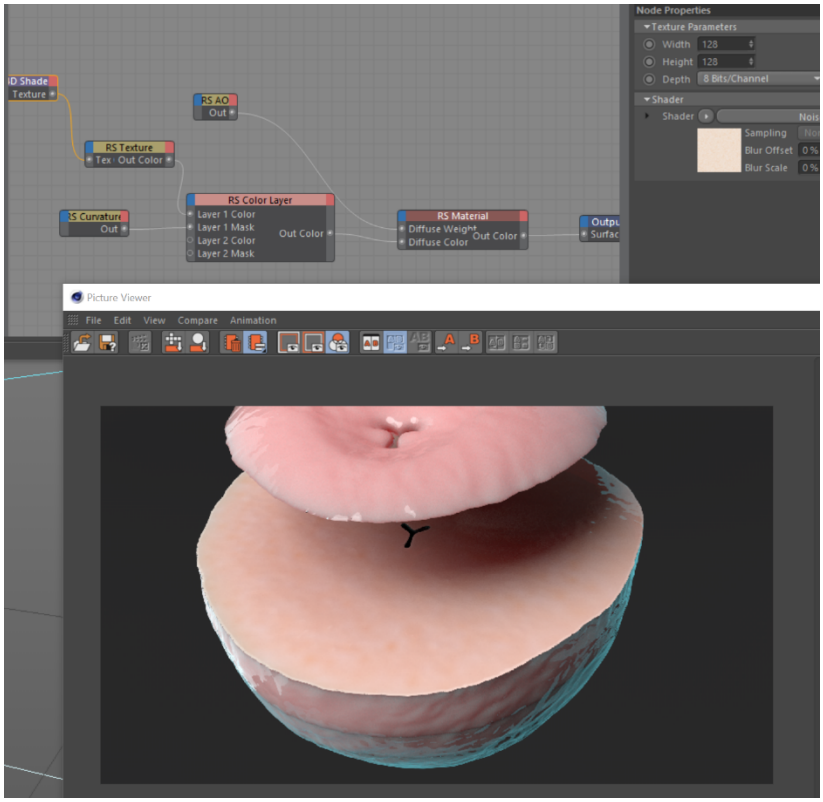

Figure 7. Redshift Material application. Redshift material nodes showing procedural creation. Text not intended to be read.

To provide the orientation and location of the prostate, an adult male 3D body model was created. A premade project of the male figure was imported onto the canvas in ZBrush to accelerate the process of modeling the male silhouette (**LightBox** > **Project** > **DemoProjects** > **SuperAverageMan.ZPR**). Using this basic mesh, additional steps were required to adequately intigrate the mesh into the animation. The preliminary animation consisted of zooming into the prostate in the pelvis, but the male body mesh had all extremities modeled which were of little importance to the location of the prostate. Using Boolean subtraction, two large rectangular prisms were appended into the Subtool Palette and were resized and relocated to cover the arms, head, and legs (**Append** > **PM3D_Cube3D1**). Before Boolean subtracting the rectangular prisms from the male body, the surface subdivisions were increased for the male body and the rectangular prisms with equal ActivePoints for all three meshes (**Ctrl** + **D**). These ActivePoints values were kept approximately equal to preserve even geometry through the Boolean subtraction process. Once appropriate placements of the rectangular prisms were completed, the meshes were combined leaving the male abdomen, pelvis, and thighs, as one mesh (**Boolean** > **Make Boolean Mesh**). To redistribute even topology and to reduce ActivePoints size, ZRemesher was used with a combination of subdividing the mesh as needed (**Ctrl** + **D**; **Geometry** > **ZRemesher** > **ZRemesher**). After the geometry was uniform and re-topologized, the male body was exported as an OBJ file (**Export** [SubTool Palette] > **Save as format: OBJ**).

Prostate Gland and Luminal Epithelium

The following scene was staged in the lumen of a prostatic duct where the camera dives into the peripheral zone of the prostate slice on screen. To create a three-dimensional representation of the prostatic duct, histological slides were used as primary reference material. In Cinema 4D, six circle splines were loaded onto the scene and distanced relatively equal distances from one another to create the shape of a tube. The **Loft** generator was used to form 2D geometry connecting all six circle splines. The six splines were placed under the **Loft** generator as 'children' and a continuous tube was created and used as the backbone of the lumen. Next, subdivision surface was used to increase the polygon count and overall smoothness of the tube geometry (**Figure 8**).

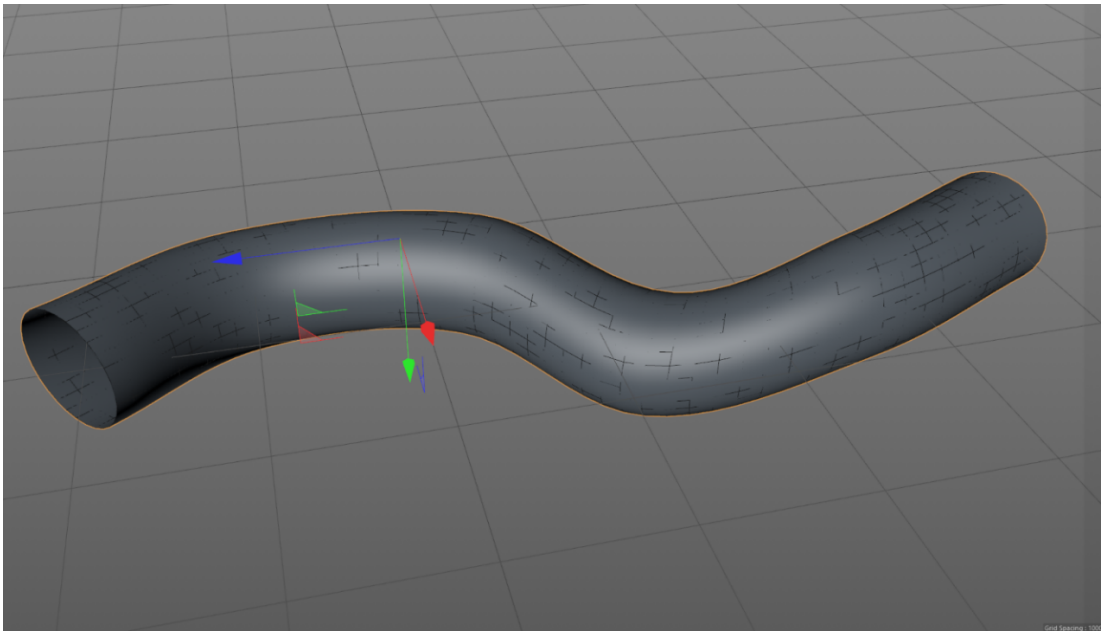

Figure 8. Creation of the prostate gland. Six splines connected to create a continuous tube.

To add organic form to the tube, all of the items on the object list were combined and turned to editable geometry (**Right Click** > **Connect Objects and Delete**). The sculpting package of Cinema 4D was used to distort the tube into the organic form of a prostate gland) (**Figure 9**).

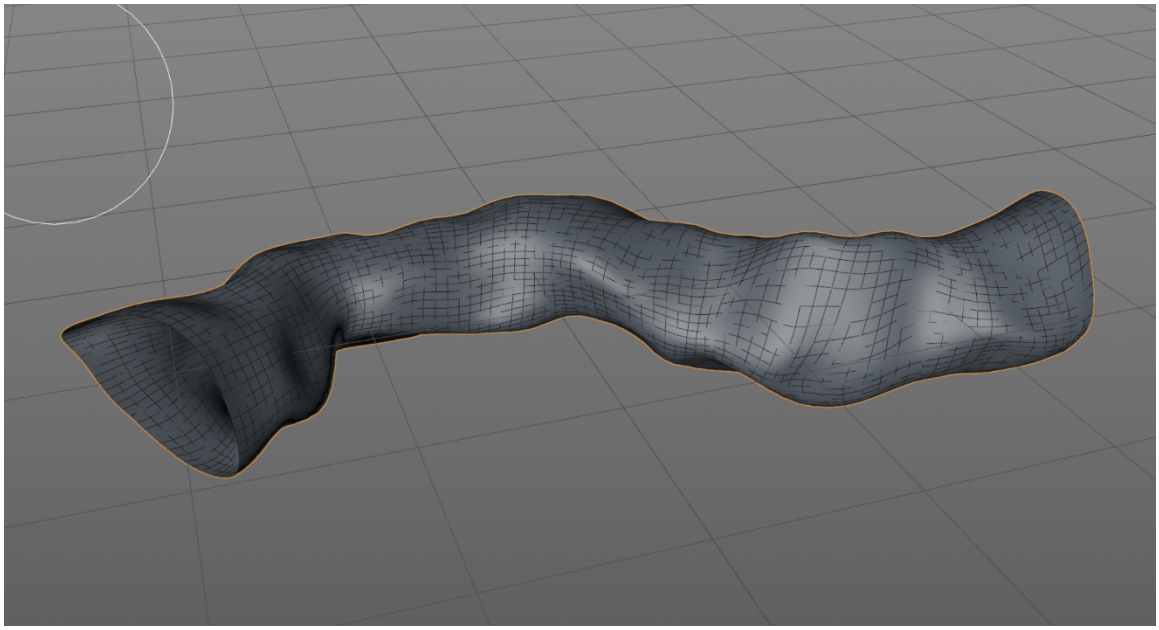

Figure 9. Modifying the lofted tube with Move in Cinema 4D. The viewport appearance of the manipulated editable tube.

After the desired shape of the lumen was achieved, spheres were added to simulate individual luminal epithelial cells. A sphere object was placed into the scene and was scaled at an appropriate size in comparison to a gland (**T** + **Left Click** + **Drag Up/Down on Screen**. The polygon count for the sphere to be cloned was reduced to allow easier Viewport manipulation. A Cloner Object was used to duplicate one hundred and sixty thousand clones of the sphere throughout the surface of the lumen mesh (**Figure 10**). The spheres were sized and distributed randomly to replicate the uneven surface of the lumen. Due to

random distribution of the clones, bare areas of the tube were seen with large gaps in between each sphere. In all visible bare areas, spheres were manually placed in small clusters to cover them from being seen from the camera. After all visible areas were covered, all of the objects in the object list were combined into one object (**Select All Objects in Object List** > **Right Click** > **Connect Objects and Delete**) A Redshift material with subsurface scattering was used to add texture to the luminal epithelial cells lining the lumen of the prostatic gland (**Create** > **Redshift** > **Materials** > **Material**) (**Figure 11**).

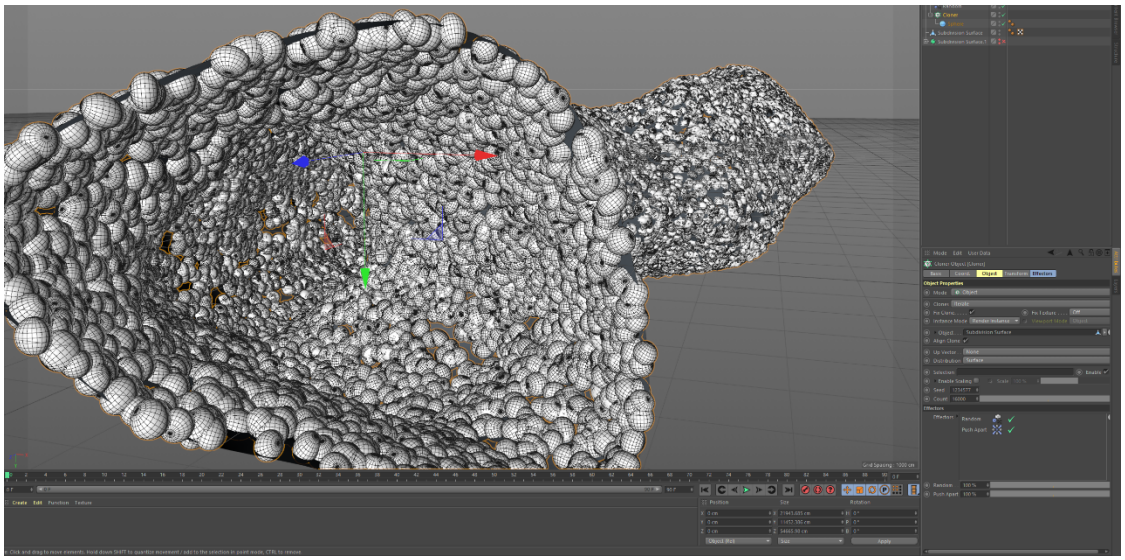

Figure 10. Cloning spheres to create individual luminal epithelium. The result of cloning one hundred and sixty thousand spheres onto the deformed lumen. Text not intended to be read.

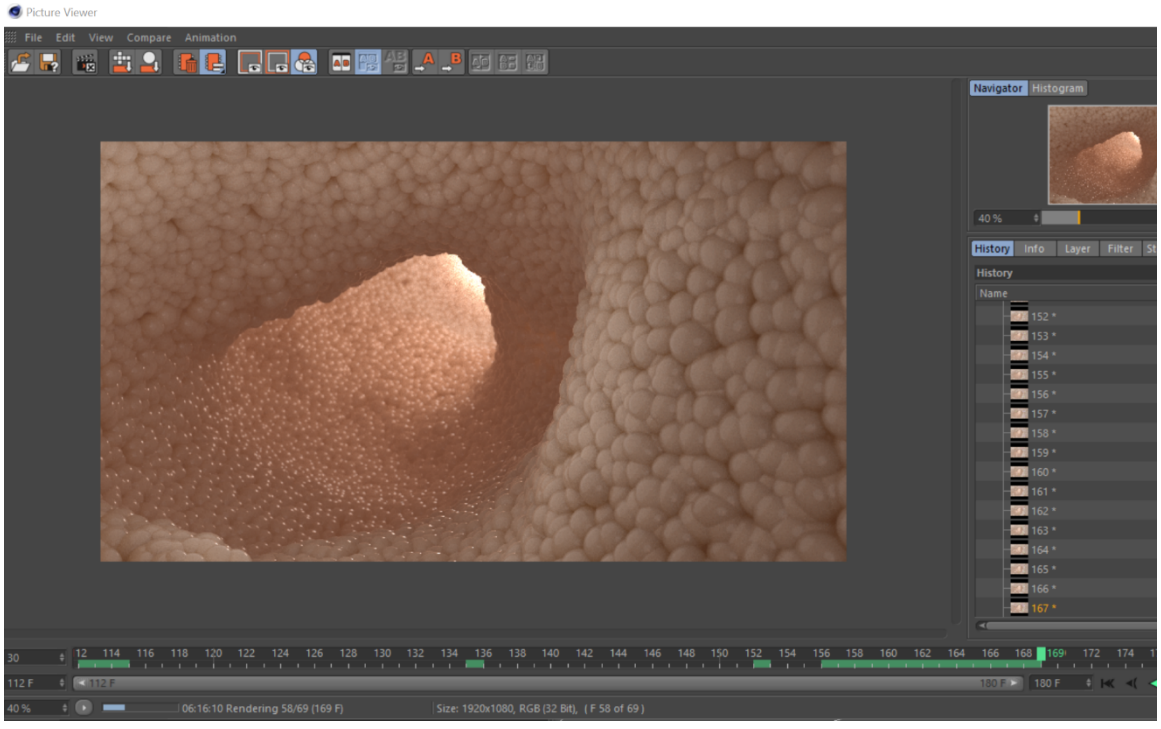

Figure 11. Redshift render of luminal epithelium material.

Modeling Bacteria in Cinema 4D

As the animation progressed, bacteria were seen swimming through the lumen of the prostatic gland. The bacteria chosen to be represented within the prostate was *E. coli* due to the fact that this strand of bacteria is commonly seen within the adult prostate. In Cinema 4D, a pill primitive was imported onto the scene and the height, width, rotation segments, and height segments were adjusted to create the appropriate dimensions of an *E. coli* bacterium. *E. coli* electron microscopy images were used as reference to depict accurate dimensions (**Figure 12**).

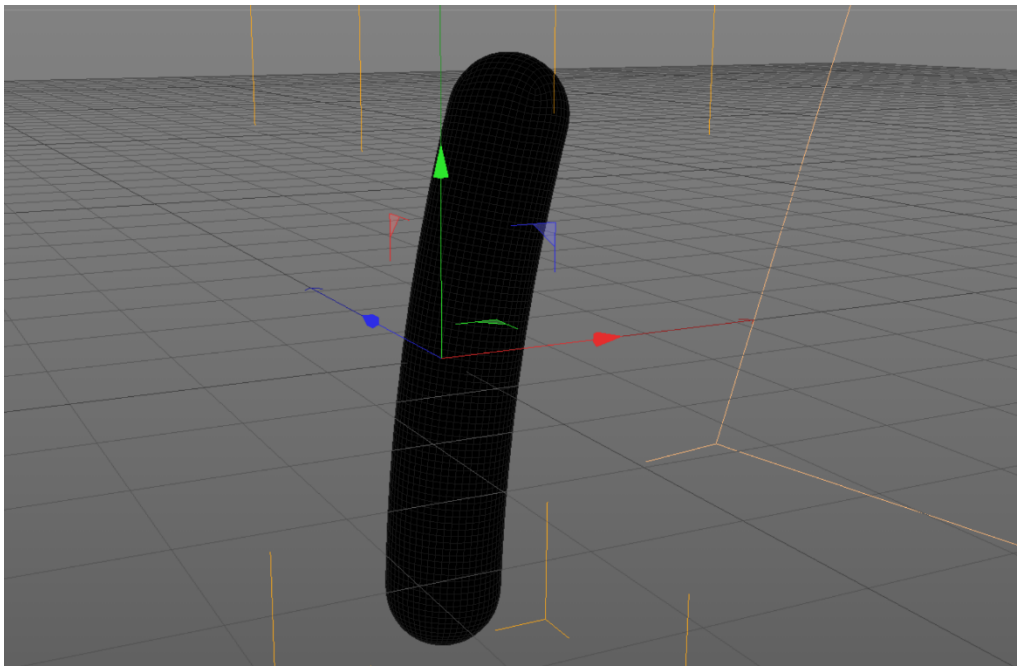

Figure 12. Viewport of the edited pill object in Cinema 4D. This viewport image shows the proportioned shape of the E. coli bacteria after referencing microscopic imaging.

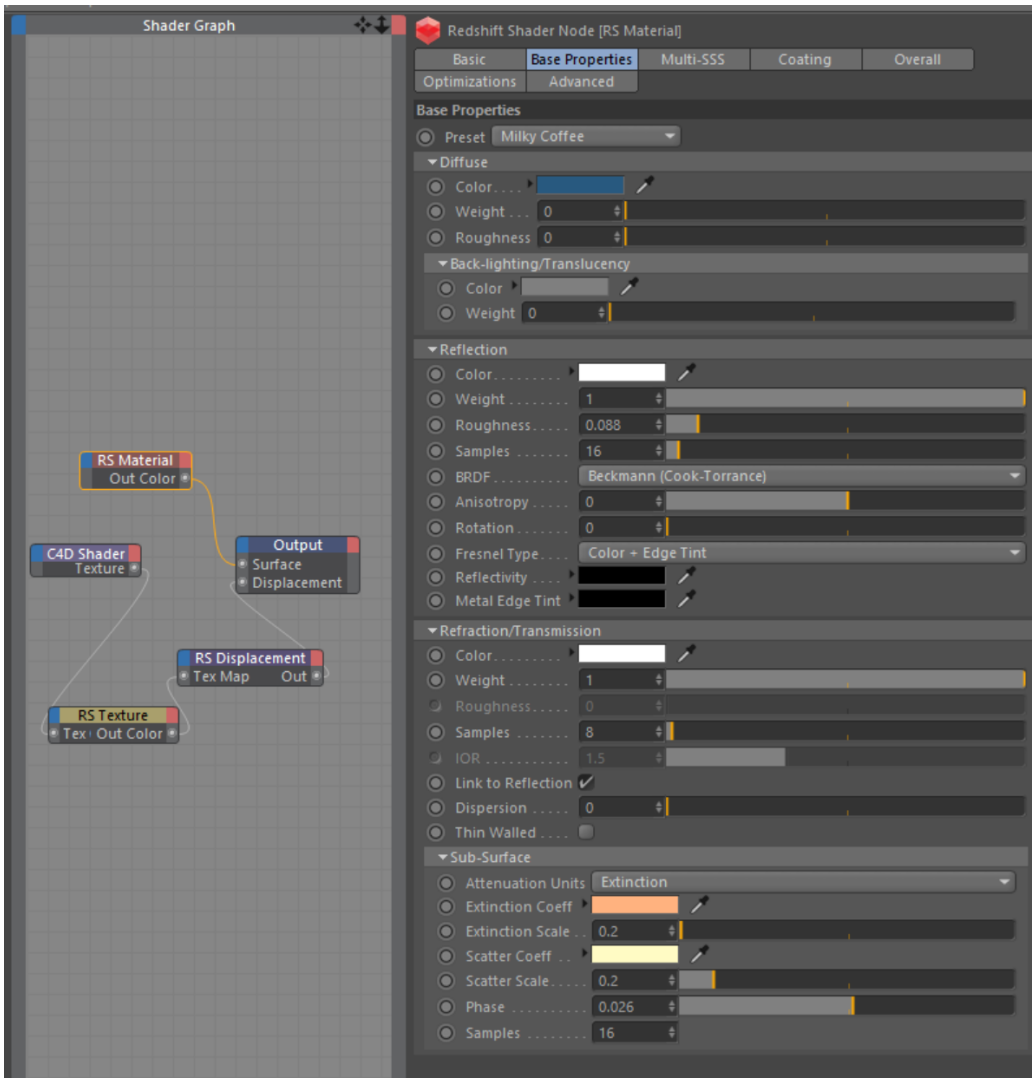

Figure 13. Material node for *E. coli*. Hierarchy of the shader graph in Cinema 4D showing Redshift material creation. Text not intended to be read.

To create cellular surface texture, a Redshift material was assigned to the pill object (**Create** > **Redshift** > **Materials** > **Material**). In the Redshift material, nodes were placed into the shader graph and adjusted to create a blue subsurface scattering material (**Figure 13**). Small hairs on the surface of the *E. coli* bacterium were also created to represent the small pili and flagella seen under the microscope. Using Redshift, a hair material was added to the object to

create small randomized hairs throughout the entire surface of the object (**Create** > **Redshift** > **Materials** > **Hair Material**). Once the hairs were created, the hair splines were swept using the Sweep generator and a circle spline with a very small radius. **Turbulence** and **Friction** MoGraph Effectors were linked to the hair materials to add kinks and frizzy characteristics (**MoGraph** > **Effector** > **Turbulence**; **MoGraph** > **Effector** > **Friction**) (**Figure 14**). The same subsurface scattering material node used for the body of the *E. coli* was added to the hair materials for the pili and flagella (**Figure 15**).

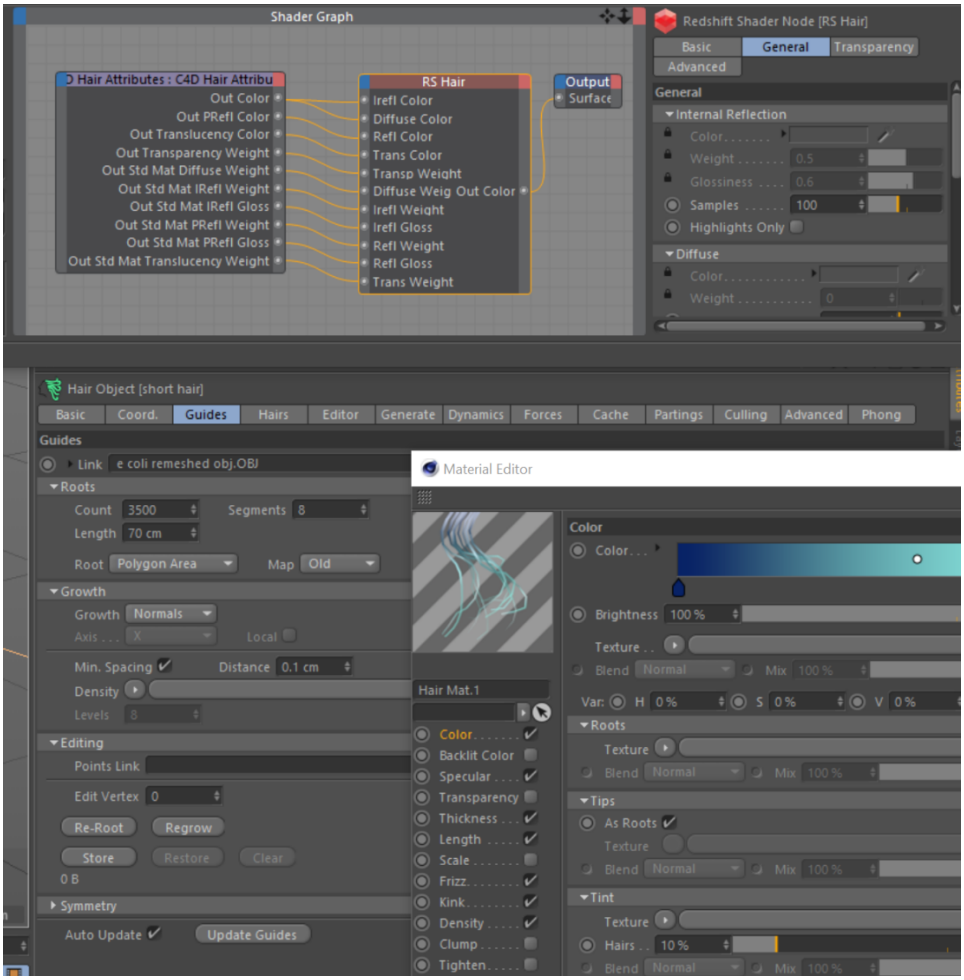

Figure 14. Screenshot of hair shader graph in Cinema 4D for pili and flagella. Text not intended to be read.

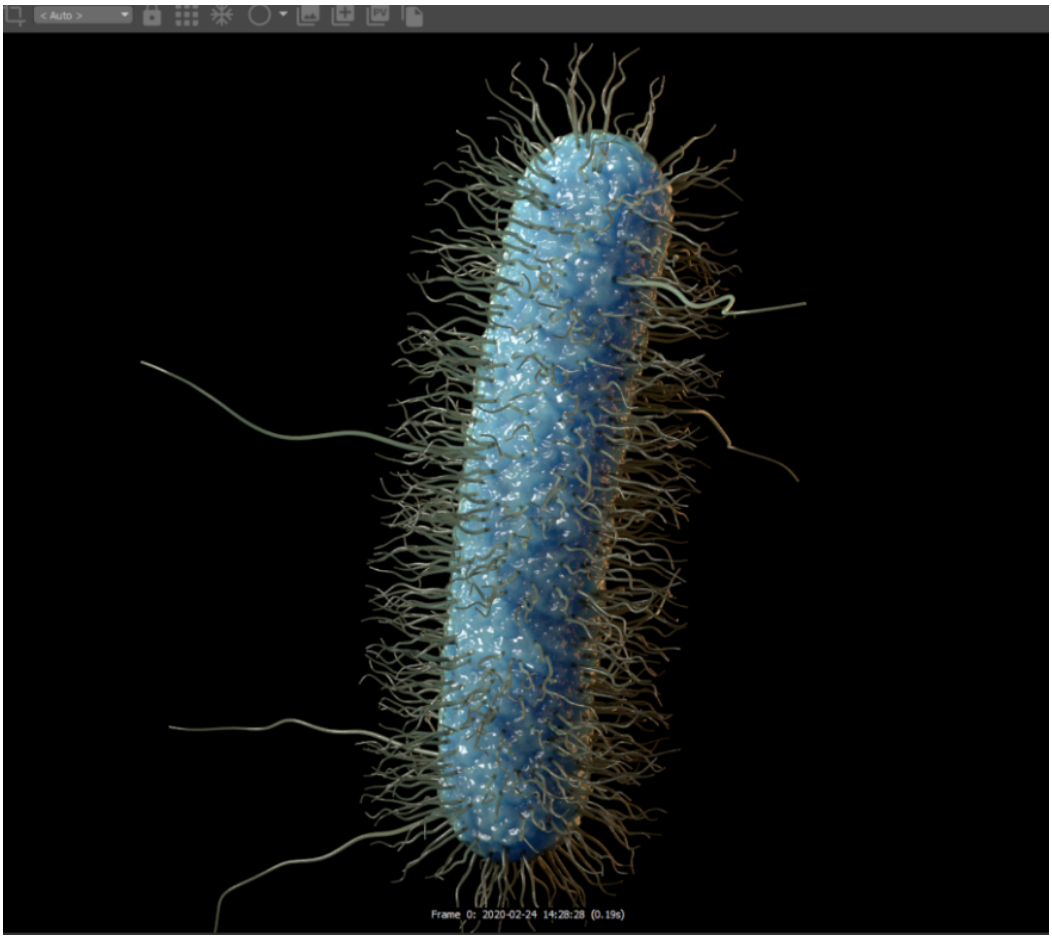

Figure 15. Rendered frame of E. coli in Cinema 4D using Redshift materials.

Creating Immune Cells

Immune cells appeared in the following scenes to depict chronic inflammation, so they were then modeled and animated. Creation of the immune cells began with creating a sphere primitive in Cinema 4D. The surface of the sphere was manipulated to create small bumps and distortions as seen in electron microscopy images. A total of three immune cells were created: macrophage, monocyte, and neutrophil. Once the rough shape for the immune cells were completed, the surface was further textured using a custom Redshift material.

This method would produce results with fewer polygons to prevent any delays or lag in the viewport.

Adjusting the Camera and Lighting in Cinema 4D

Next, the default camera in Cinema 4D was rigged to become an easily controllable and adjustable object within the scene. First, a Target Tag was applied to a Redshift Cinema 4D Camera (**Redshift** > **Cameras** > **Standard**; **Tags** > **Cinema 4D Tags** > **Target**). The target chosen for the Target Tag was a Null object. A horizontal circle spline was used as the rotation for the camera rig. User Data was activated on the Null Object to create Float Sliders to adjust the target height, distance, rotation, Move X, Move Y, and Move Z of the camera rig. The camera rig User Data was dragged onto the Expressor Editor and the node options for the target height, distance, rotation, Move X, Move Y, and Move Z were added to the User Data node. The corresponding nodes of the camera rig were then linked to the circle spline and the Target Tag to control the positions via sliders in the User Data. The camera was keyframed for each scene according to the approved animatic.

To light the scenes, Redshift lights were used in combination with default Cinema 4D lights (**Redshift** > **Lights** > **Area Light**/**Dome Light**). Models were animated using deformers and then keyframed in Cinema 4D. After the scenes were rendered using Redshift, the frames were saved as PNG sequences due to their small size and lossless characteristics. The PNG sequences were then imported into Adobe After Effects for compositing the frames into a moving

animation. Further color adjustments, time stretching, and transitions were edited in After Effects.

RESULTS

Animation Storyboards and Rendered Stills

A set of black and white storyboards (**Figures 16-33**) were developed in Photoshop to portray the 3D animation in a 2D format, also known as the animatic. The animatic would serve to develop the imagery being displayed as well as the pacing of the narration.

The final animation video file was 3 minutes and 55 seconds in length (**Figures 34-43**).

Figure 16. Zoom into the pelvis; the male silhouette fades completely and the prostate remains.

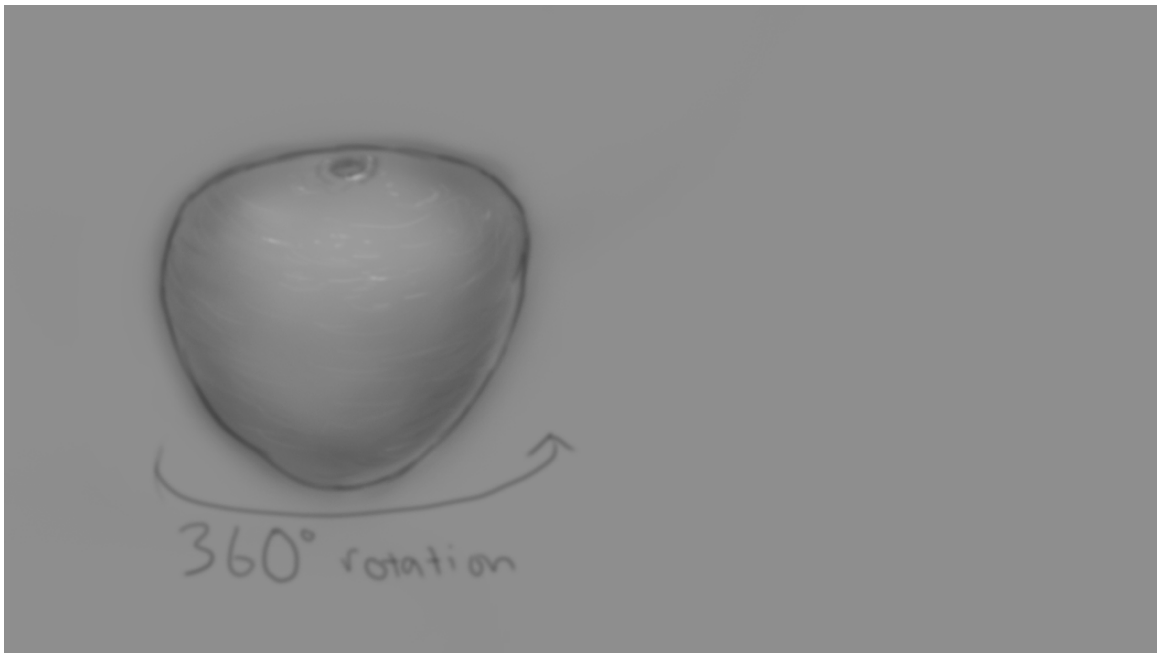

Figure 17. Prostate rotates 360º to display its form and shape.

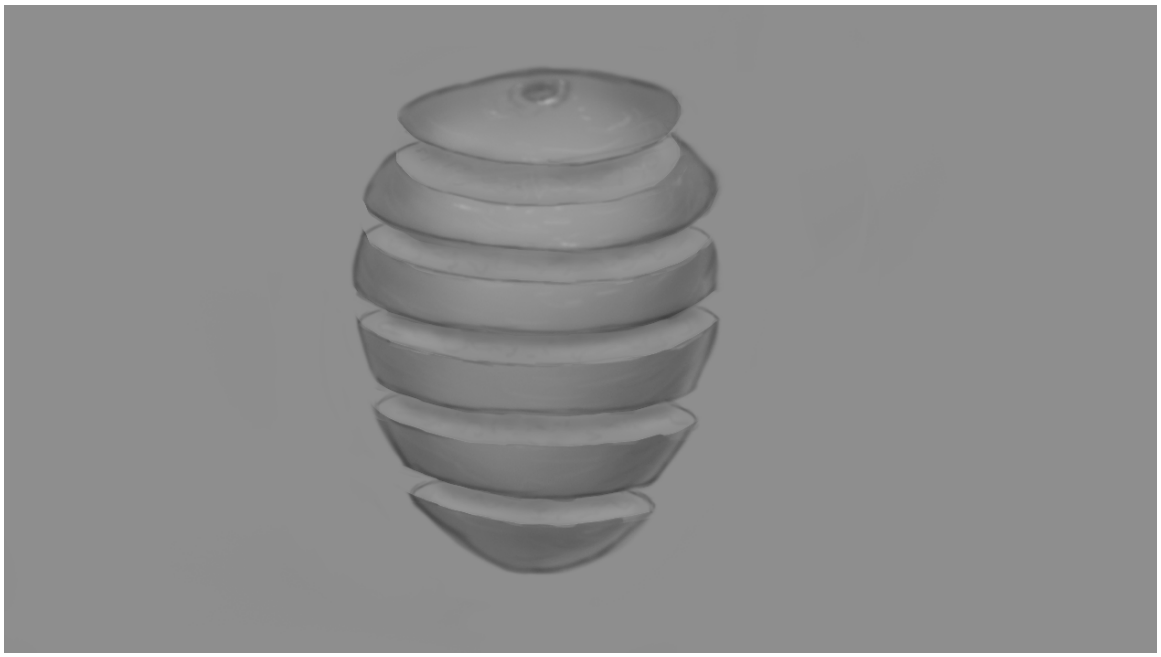

Figure 18. The prostate is sectioned into several slices to portray the method used by pathologists when studying the histology of the prostate.

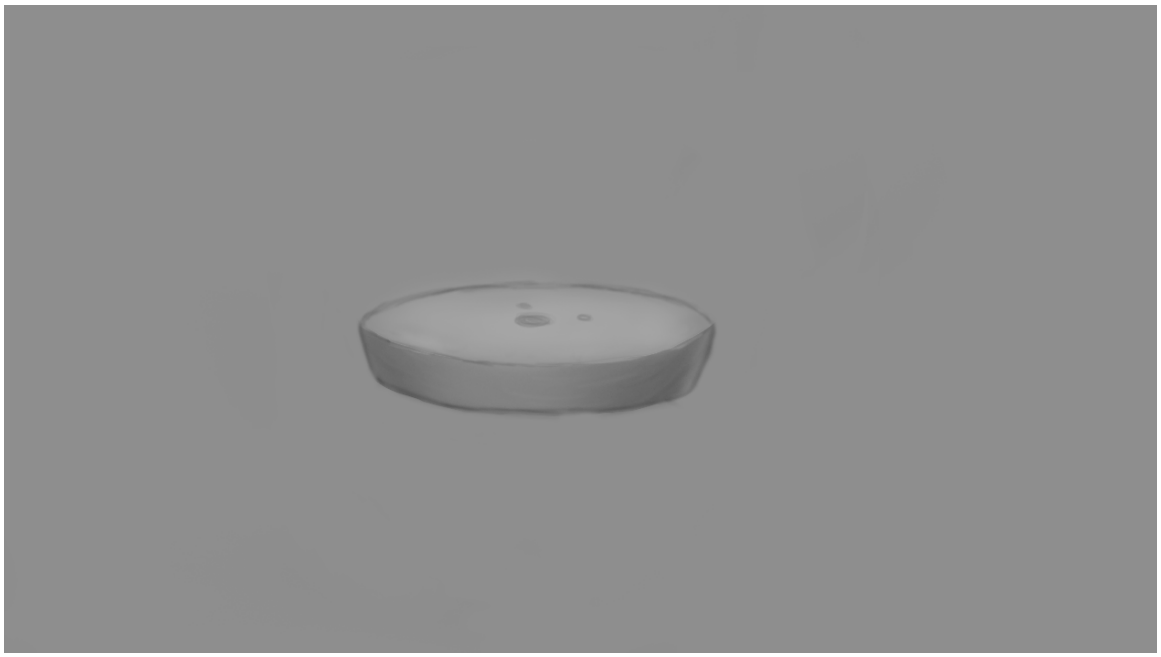

Figure 19. One slice of the prostate remains as the other slices are removed from the scene

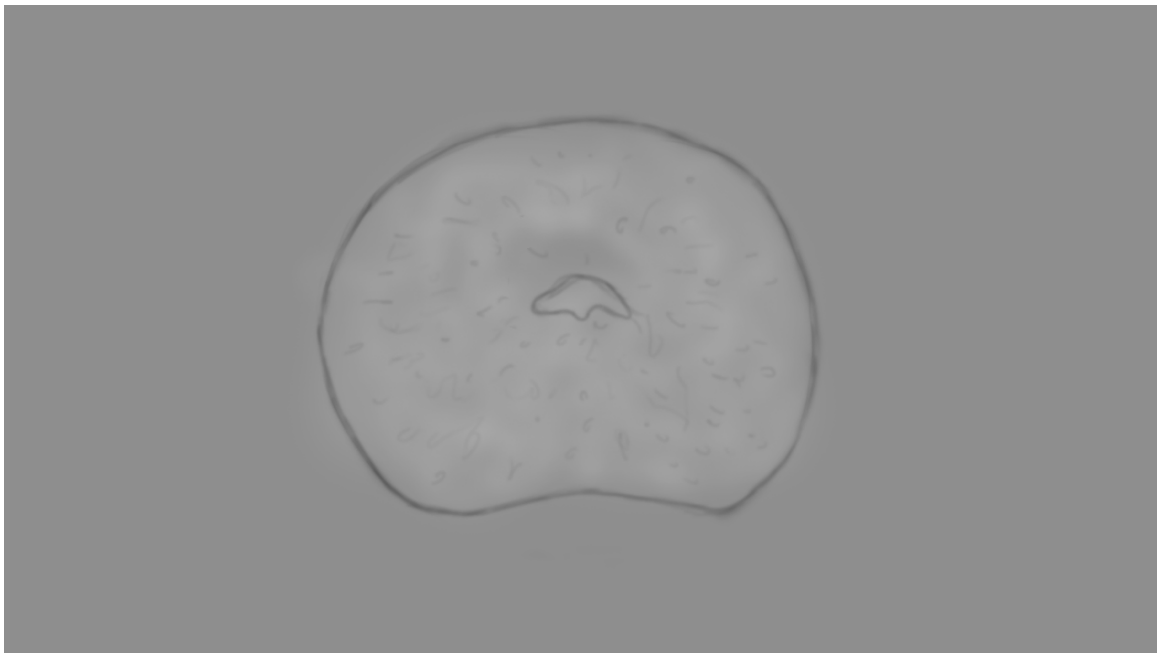

Figure 20. Single slice is oriented to be parallel to the camera and then divided into four quadrants.

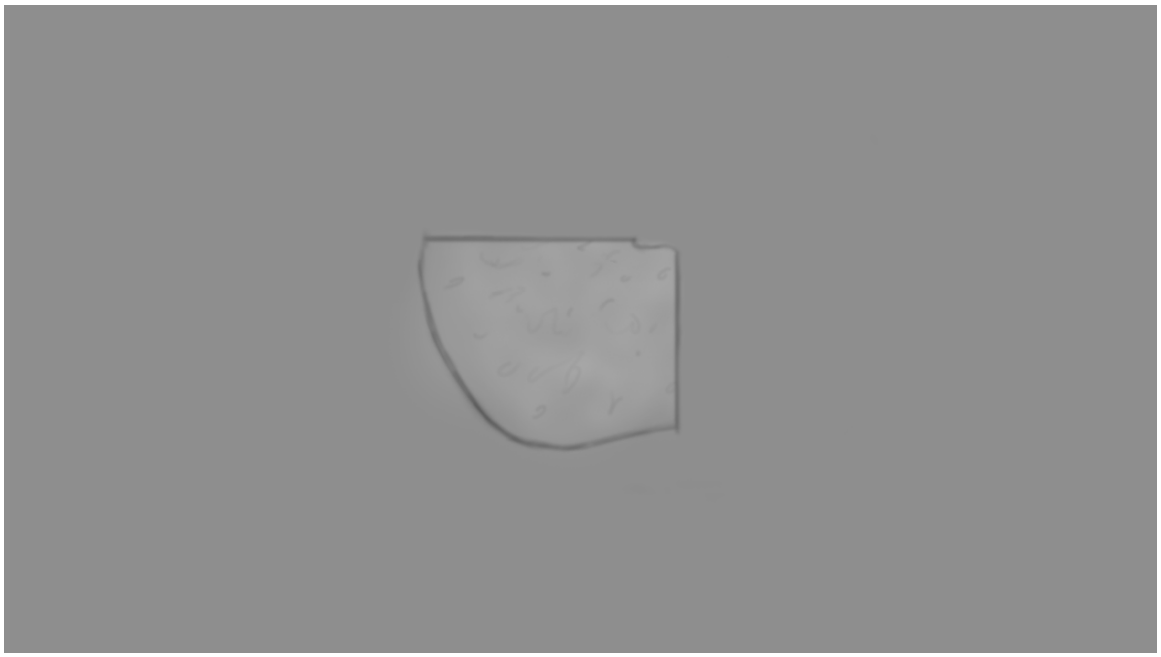

Figure 21. One quadrant of the slice remains and the three remaining slices are removed from the scene.

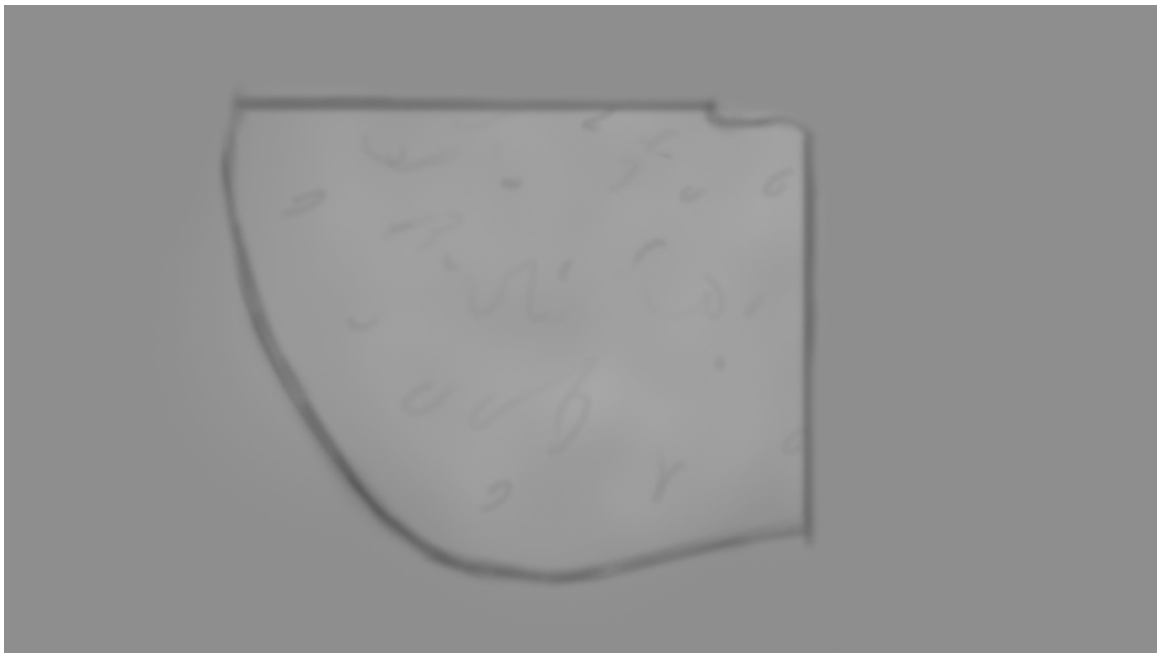

Figure 22. A single quadrant of the slice is brought close to the camera and is held in place.

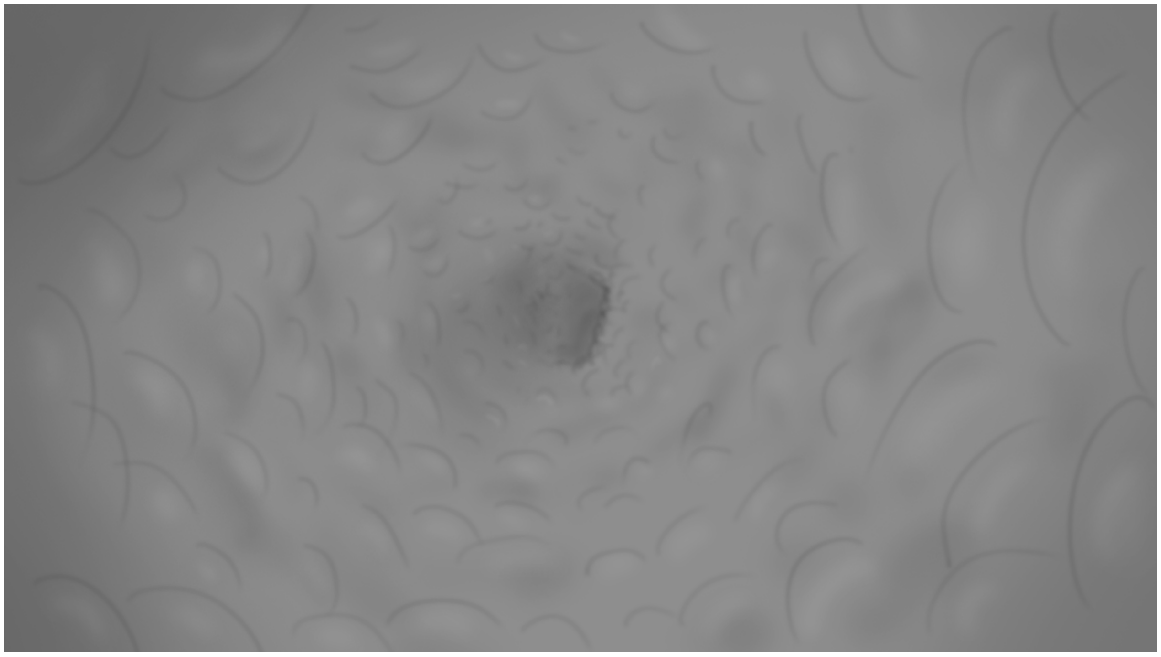

Figure 23. The camera zooms into the quadrant of prostate into the lumen of a gland.

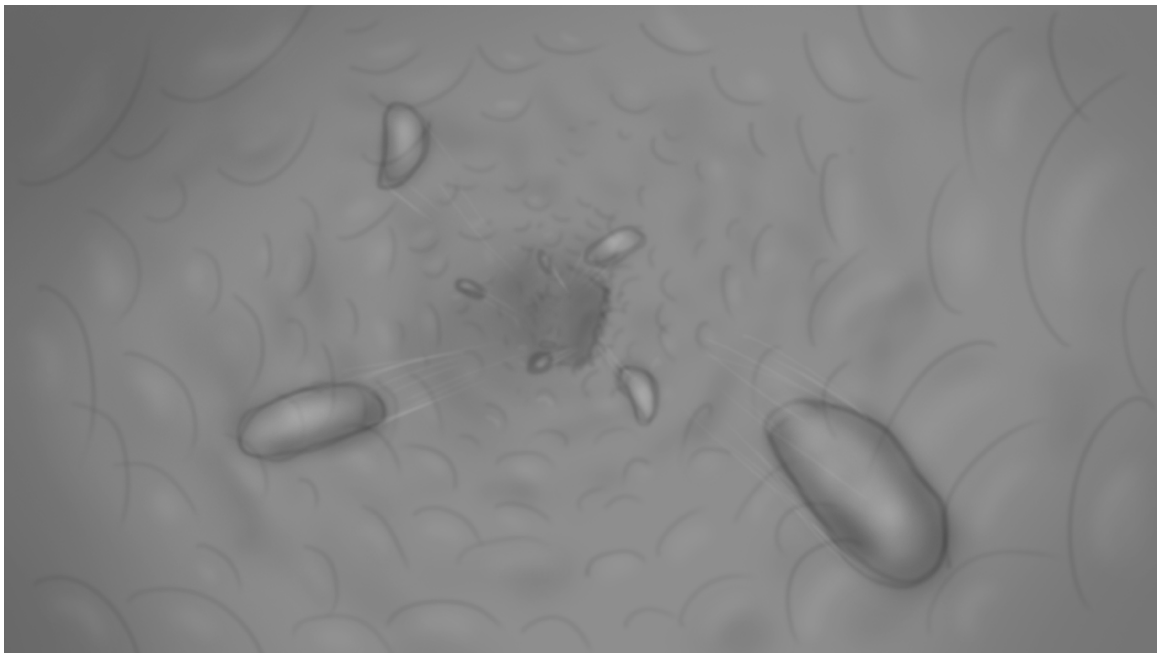

Figure 24. E. coli are seen traveling through the lumen.

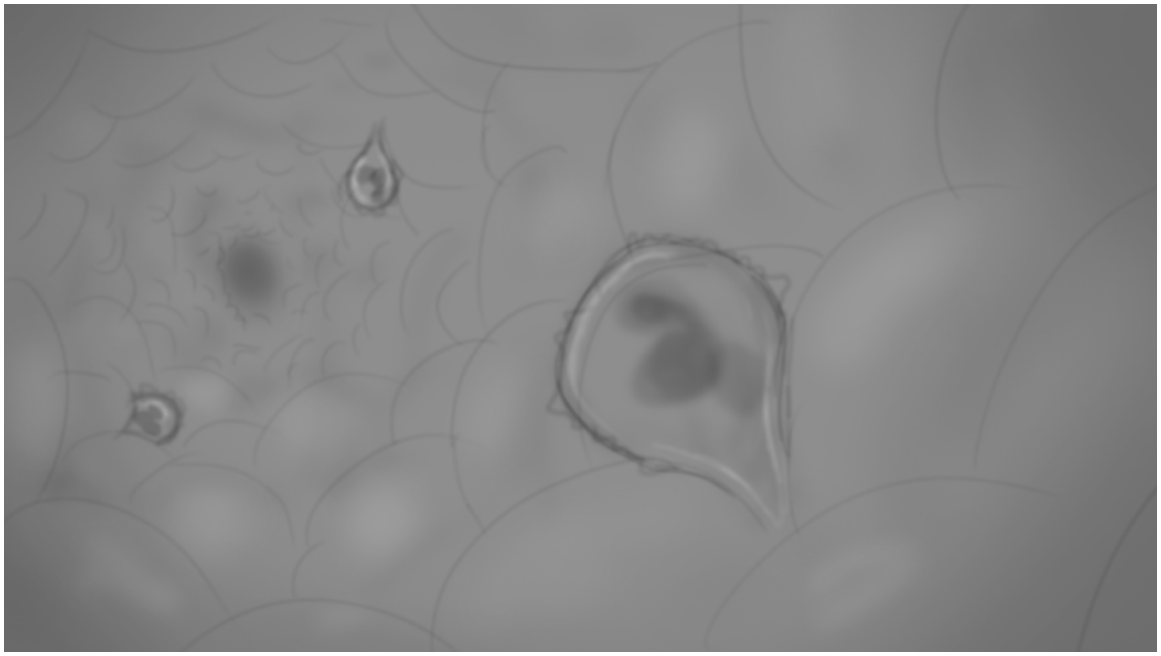

Figure 25. Immune cells detect the presence of E. Coli and begin to mobilize into the lumen.

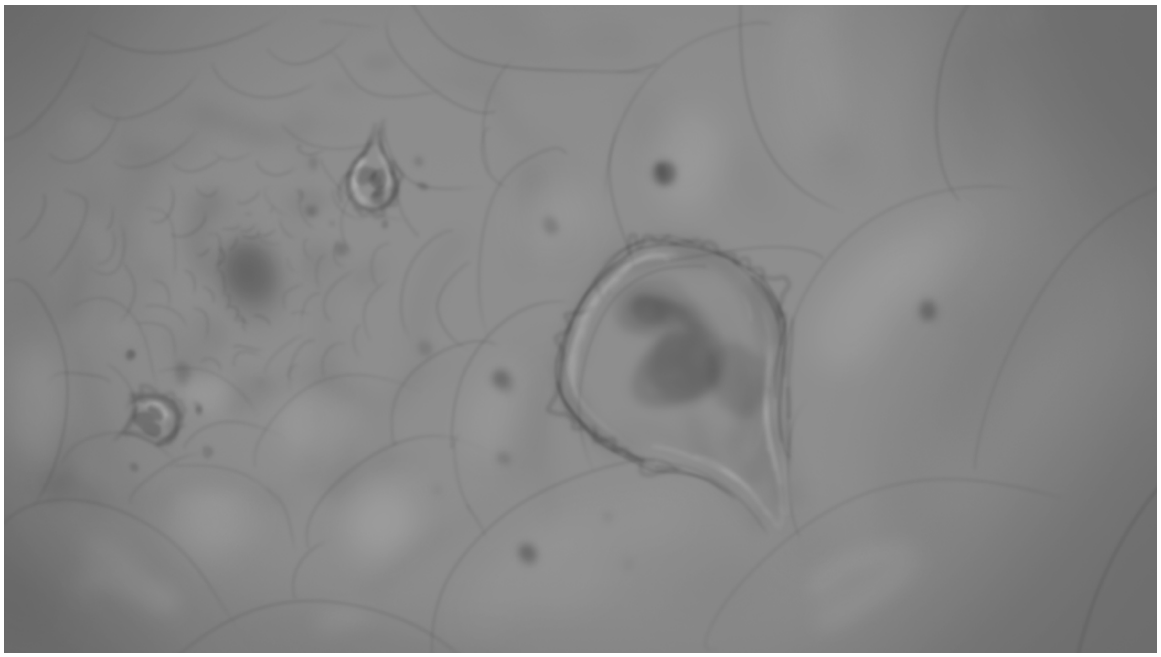

Figure 26. As immune cells travel into the lumen, they release cytokines to alert nearby immune cells of invading bacteria. Reactive oxygen species are also actively released by the immune cells during this time.

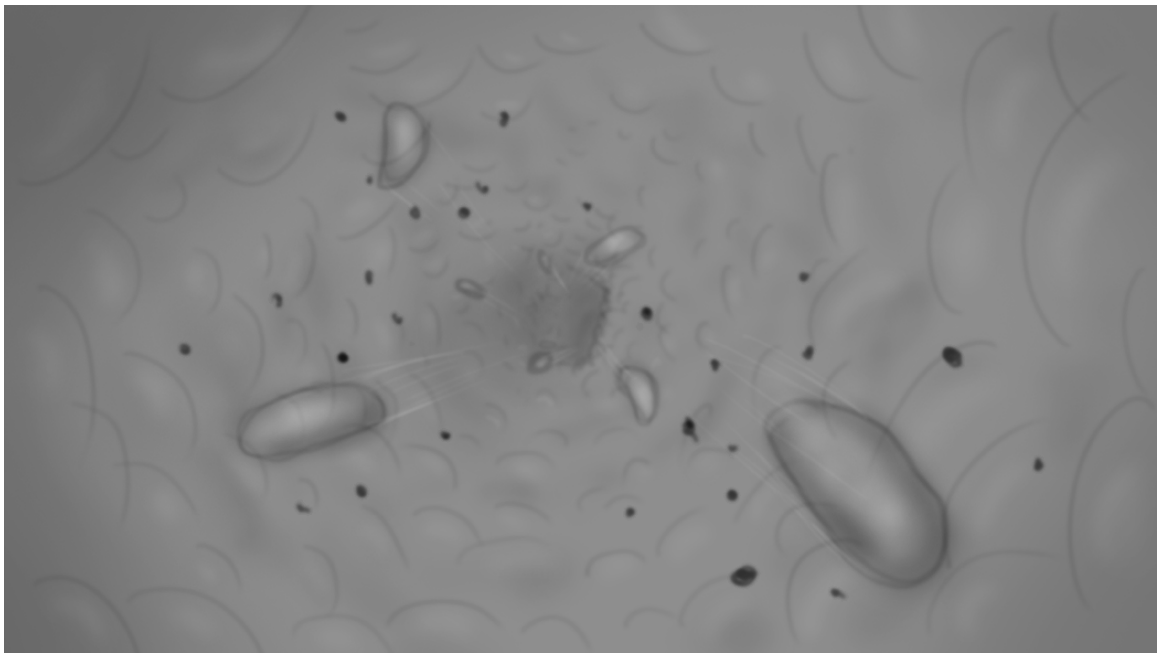

Figure 27. As bacteria travel through the prostate gland, they release toxins that may be harmful to the luminal epithelium.

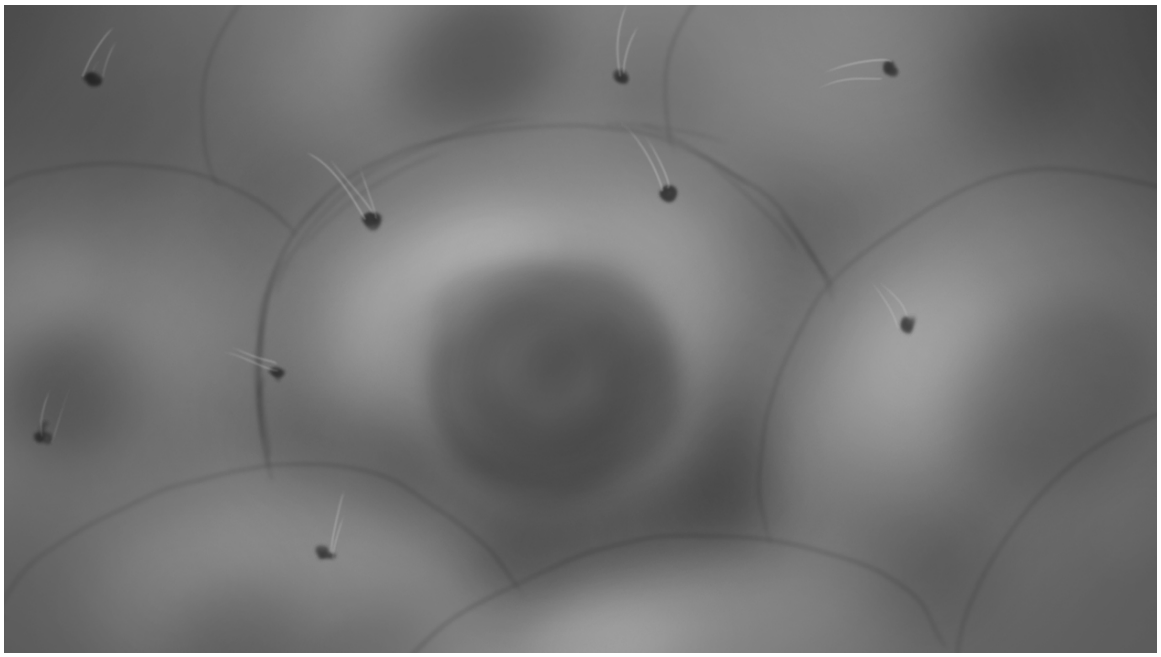

Figure 28. The camera pans towards luminal epithelium as reactive oxygen species and bacterial toxins enter the cells.

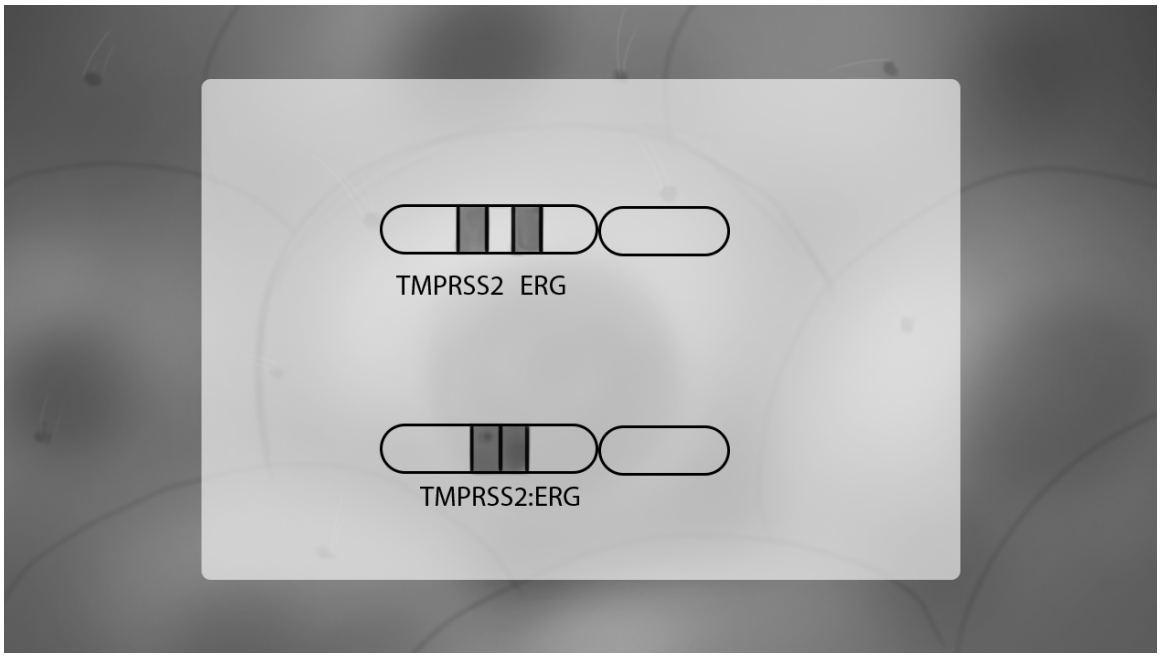

Figure 29. A 2D schematic of the luminal epithelial cell's DNA depicts the potential damage induced by the reactive oxygen species and the bacterial toxins.

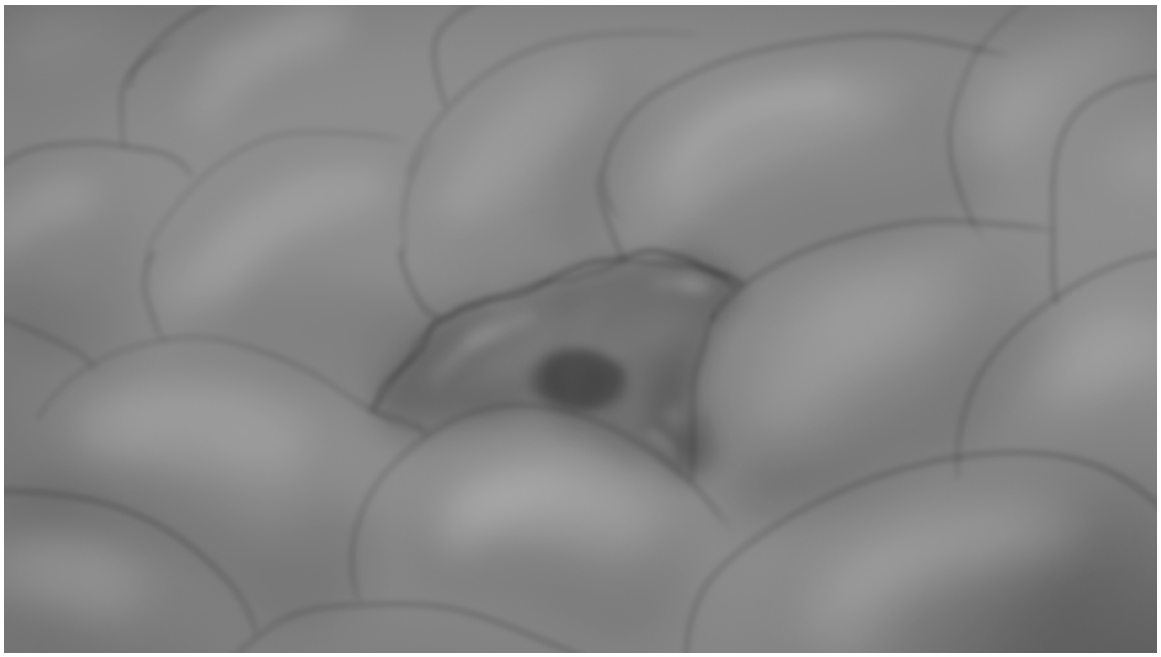

Figure 30. The camera then goes back to the cell absorbing the reactive oxygen species and bacterial toxins as it becomes atrophic and withered in appearance.

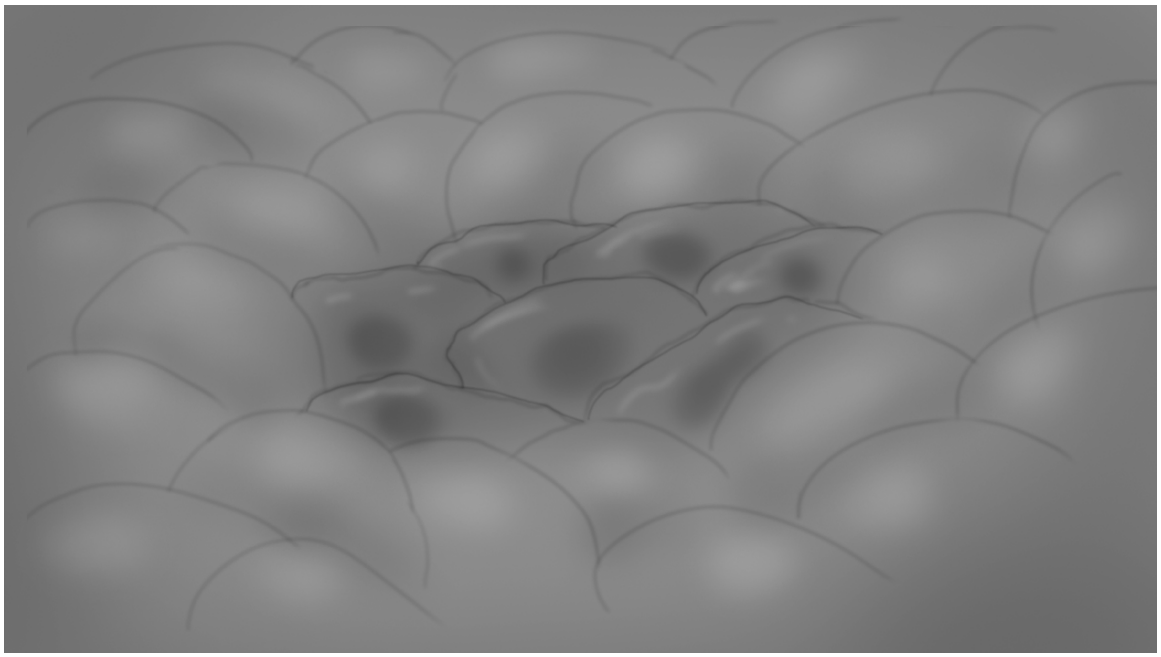

Figure 31. The small atrophic cell then begins to divide and push away normal luminal epithelial cells.

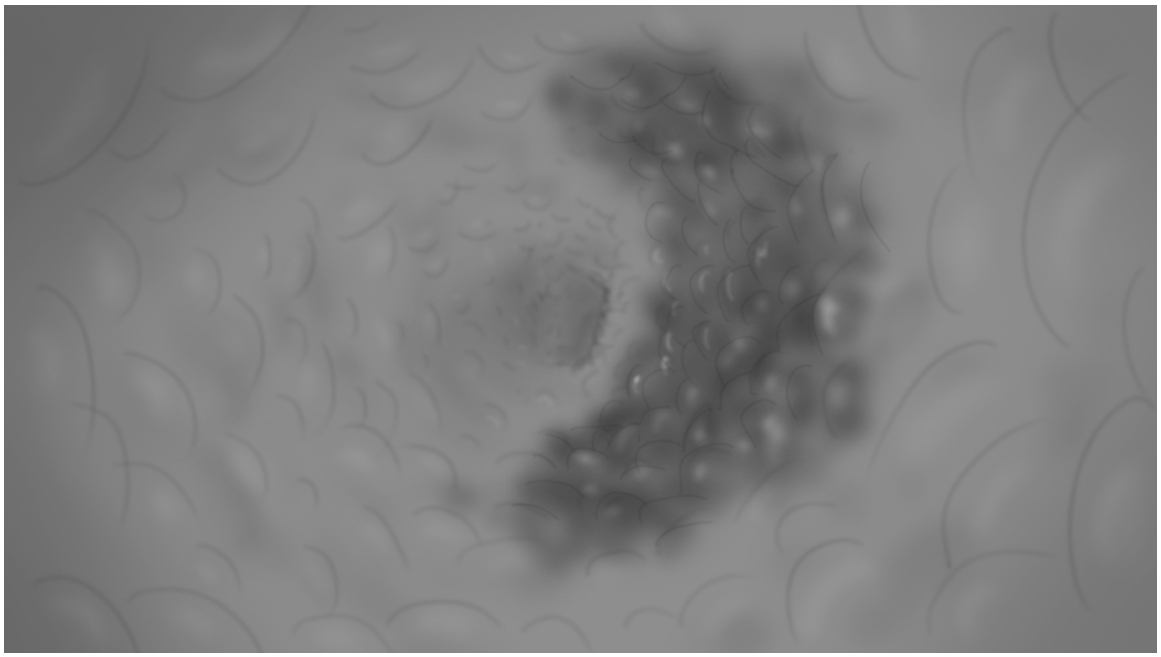

Figure 32. As the viewer zooms out from the small cluster of atrophic epithelial cells, a large portion of the luminal epithelium can be seen with large patches of atrophic lesions.

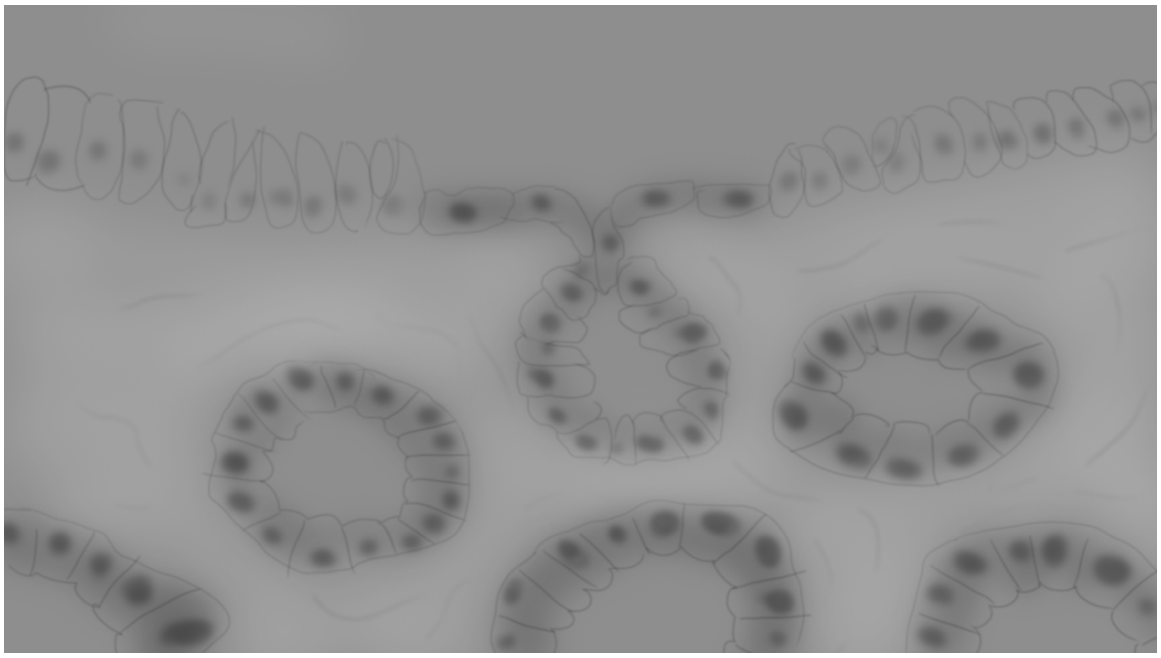

Figure 33. A cross-section of the atrophic lesion is made visible as the camera moves away from the lumen. A histological microscope slide of an ERG+ lesion will fade onto this 3D modeled scene.

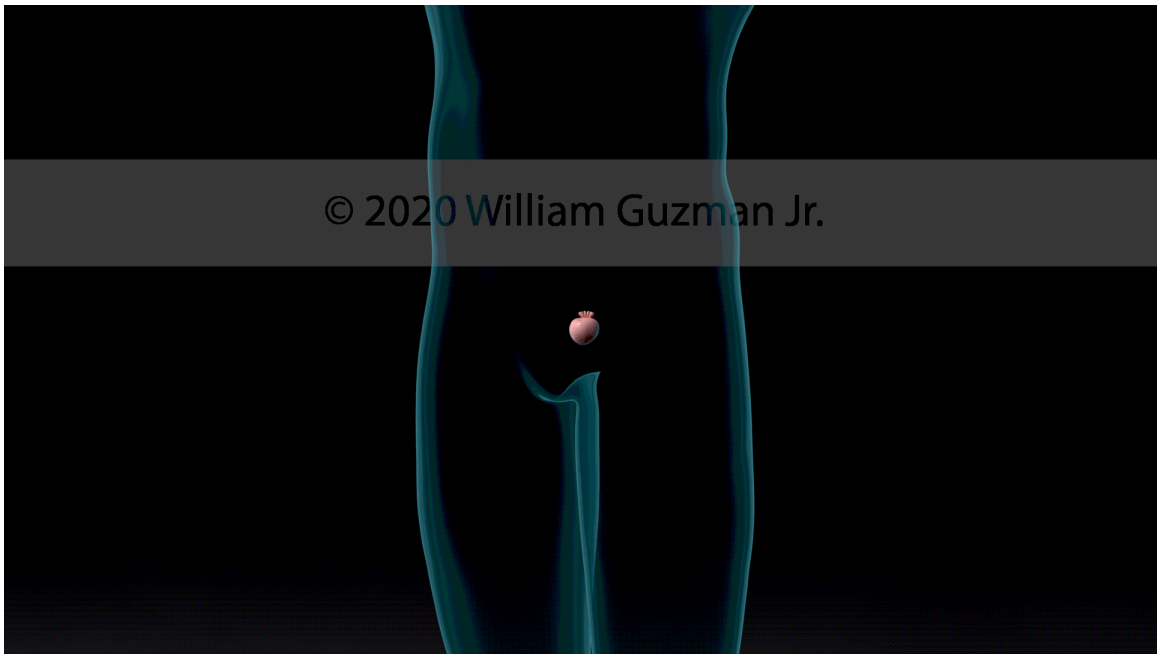

Figure 34. Animation still. Opening scene.

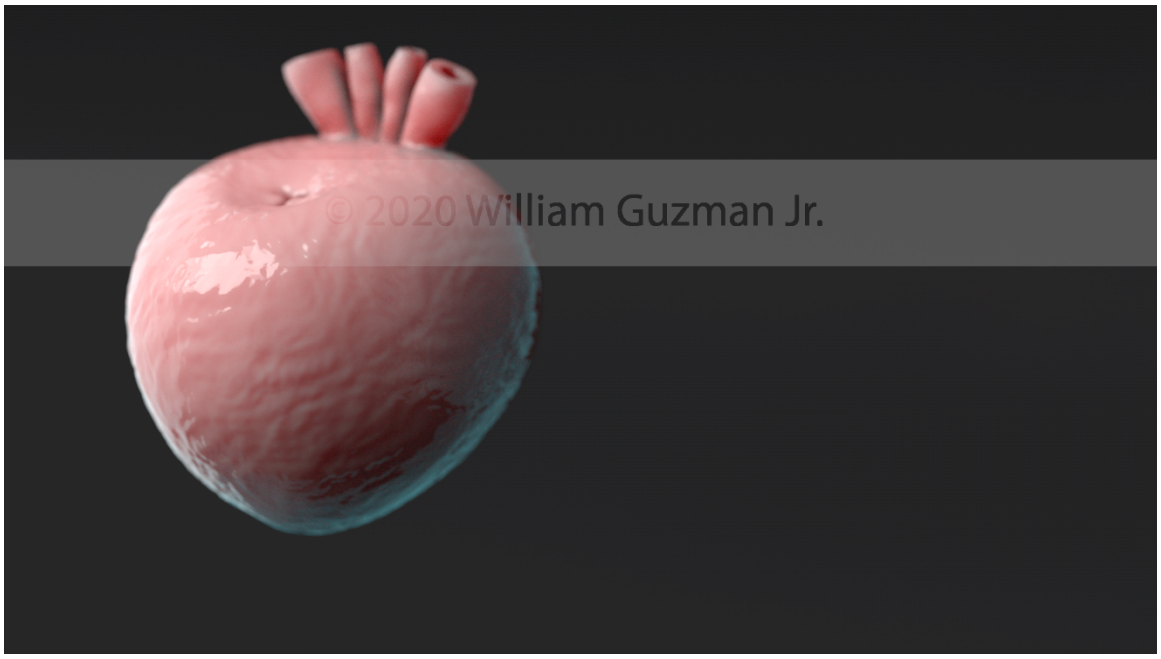

Figure 35. Animation still. Prostate is brought into focus.

Figure 36. Animation still. Slicing of the prostate.

Figure 37. Animation still. Slices are removed.

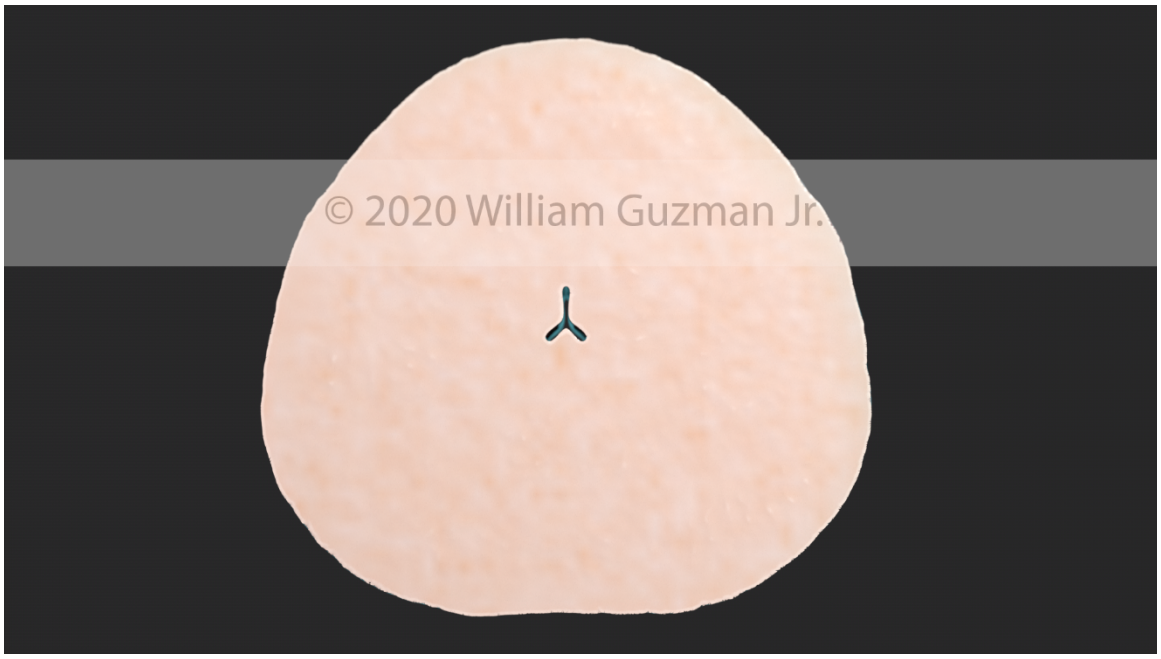

Figure 38. Animation still. Remaining slice is brought into focus.

Figure 39. Animation still. Viewer is within a prostatic gland.

Figure 40. Animation still. Camera pans over to normal luminal epithelium.

Figure 41. Animation still. E. coli is seen swimming past the epithelium.

Figure 42. Animation still. An immune cell releases cytokine in response to bacterial presence.

Figure 43. Animation still. Mutated luminal epithelial cell becomes atrophied and divides uncontrollably.

Access to Assets

Access to the animation from this thesis can be viewed at http://labs.pathology.jhu/sfanos/ and https://plasmavisuals.com/. The author may be reached through the website of the Department of Art as Applied to Medicine at https://medicalart.johnshopkins.edu/.

DISCUSSION

Project Goals

The primary goals of this project were to fill a visual void in communicating pathological prostate cancer data and to create a 3D animation to visualize a proposed mechanism of disease for precursor lesion development. Another goal was to illustrate the didactic method of using novel histological datasets within a 3D animation to effectively understand 2D microscope slide evidence. The results of this project were intended to educate graduate students, prostate cancer researchers, and non-prostate cancer researchers by providing a didactic visual to understand this new hypothesis.

Challenges Encountered During the Project

The goal of the animation was to communicate a visually challenging proposal to an audience that were non-prostate specialists. This proved challenging in regards to writing a narrative that succinctly explains the role of the microbiome within the context of chronic inflammation within the prostate to researchers with little familiarity to the prostate. Initially, a script for the animation was developed that exceeded four and a half minutes.

Another challenge faced during the completion of this animation was the limited computing power needed to render the final animation. When rendering through Cinema 4D, computer generated images are calculated using the computer processing unit (CPU). Cinema 4D rendering is a multi-threaded process that uses cores in the computer's CPU. Rendering on the department

Apple iMac with a CPU that has 4 cores using Cinema 4D's built-in Physical rendering engine is time consuming and would have taken over three weeks to render the final animation. Redshift, a third-party rendering engine for Cinema 4D, was chosen for its optimized rendering times. Redshift has the capability to render 3D computer generated images by using the graphics processing unit (GPU) of the computer instead of the CPU. To use Redshift, the computer must have: a minimum of 8GB of system memory, Windows OS 7/8/10 64-bit or MacOS Sierra, and a NVidia GPU (which is no longer supported on MacOS after High Sierra OS) with CUDA compute capability 6.0 or higher with 8GB of VRAM. VRAM, or video random access memory, is typically used to store image data that is displayed by the computer, but can also be used for accelerated biased rendering when using 3D graphics programs. To use Redshift, a computer with the necessary specifications was built. The graphics processing units chosen were two ASUS ROG Strix GeForce RTX 2080 ti models with 11GB of VRAM each. This amount of GPU VRAM allowed me to use Redshift in Cinema 4D to efficiently render the 3D animation.

Accessibility

To further educate audiences within the research field, this animation will be accessible on the *Johns Hopkins Medicine Pathology: The Sfanos Laboratory* webpage. The user can revisit the website at their own leisure to view the 3D animation. At the end of the animation, a list of references will be provided for the viewer to review. The animation will be posted on YouTube and then linked

onto *The Sfanos Laboratory*'s website. This will allow the animation to use closed captions for viewers that prefer to read subtitles.

Future Directions

With the completion of the 3D precursor lesion development animation, the viewer will have a clear understanding of the new hypothesis for prostate cancer in the context of bacterial infection and chronic inflammation. The next step for this project is to delve deeper into each biological and cellular process that were briefly stated in the animation. By representing these complex and visually challenging molecular topics, viewers will be provided with more evidence to understand this recently proposed prostate cancer pathogenesis model.

APPENDIX A

Learning Objectives:

After viewing the 3D animation, the viewer will:

- Recognize histological structures of the prostate.
- Visualize novel cancer datasets from prostatectomy specimens.
- Understand the proposed development pathway for prostate cancer precursor lesions.
- Identify the suspected contributors to prostate cancer.
- Understand the resulting luminal epithelium disruption caused by supposed epithelial cellular mutations.
- Comprehend the importance of the microbiome within the prostate.
- Understand the negative effects caused by chronic inflammation.

APPENDIX B

"Visualizing Prostate Cancer Precursor Lesion Development" Script

Prostate cancer is one of the most common malignant neoplasms among men in western countries. The only known risk factors for prostate cancer are advanced age, family history, and African ancestry. Genetics, diet, and other lifestyle-related factors may also play a role. Recently, chronic inflammation has been linked to the growth and development of several solid cancers and may contribute to prostate carcinogenesis.

Studying the histology of the prostate offers pathologists valuable insights into the possible pathogenesis of prostate cancer. Within the prostate, are small compound tubular alveolar ducts known as: prostatic glands. These glands are made of pseudostratified columnar luminal epithelial cells and simple squamous basal cells, surrounded by a stroma of connective tissue and smooth muscle.

In a normal prostate, the glandular luminal epithelial cells have very low cellular turnover and rarely proliferate. Inflammation in the prostate is associated with the development of proliferative inflammatory atrophy (PIA), a proposed precursor lesion to prostate cancer development. Unlike normal prostatic epithelial cells, luminal cells involving PIA have high cellular turnover and are highly proliferative.

As foreign bacteria invade the glands, immune cells such as neutrophils, macrophages, and monocytes, quickly begin to populate the lumen and release cytokines. This inflammatory state drives immune cells to produce reactive oxygen species (ROS) and reactive nitrogen species (RNS) that may cause DNA damage and DNA breaks. In addition, the invading bacteria can produce genotoxins, such as colibactin present in *E. coli*, that may also induce DNA damage in luminal epithelial cells.

When inflammatory oxidants and/or bacterial genotoxins leads to DNA breaks, abnormal gene fusions may result. Transmembrane protease serine-2 (TMPRSS2) is a protein regularly expressed and driven by androgen receptor signaling within the luminal cells of the prostate. Along the same chromosomal strand of DNA is the gene for erythroblastosis virus E26 oncogene homolog (ERG), a known oncogene. In normal functioning luminal epithelial cells, ERG is not expressed. However, recent evidence has shown that in about 50% of prostate cancer cases in the US, the promoter region of the TMPRSS2 gene has become fused to the coding region of the ERG gene; causing cells to express the ERG oncoprotein. It is hypothesized that genomic damage caused by infections and inflammation promote the formation of the TMPRSS2:ERG gene fusion, possibly playing a very early and not yet well understood role in the development of prostate cancer.

The ERG expressing cells replicate and displace the Erg negative luminal epithelial cells in the PIA lesion. These atrophic cells release pro-inflammatory

cytokines and other acute inflammatory proteins to further increase immune cell count within the glands. At some point, perhaps with the acquisition of additional genomic and/or epigenomic alterations, these Erg expressing cells invade the basement membrane. Once the luminal cells infiltrate the stroma, the basal cells are no longer maintained, and the Erg expressing cells are now consistent with prostate adenocarcinoma. These cancer cells then form smaller irregular glands within the stroma of the prostate as seen in histological findings.

REFERENCES

Aaron, Latayia, Omar E. Franco, and Simon W. Hayward. "Review of Prostate Anatomy and Embryology and the Etiology of Benign Prostatic Hyperplasia." *Urologic Clinics of North America* 43, no. 3 (2016): 279–88. https://doi.org/10.1016/j.ucl.2016.04.012.

Amis, E. Stephen. "Anatomy and Physiology of the Prostate." SpringerLink. Springer, Berlin, Heidelberg, January 1, 1994. https://link.springer.com/chapter/10.1007/978-3-642-84431-7_8.

De Marzo, Angelo M., Elizabeth A. Platz, Siobhan Sutcliffe, Jianfeng Xu, Henrik Grönberg, Charles G. Drake, Yasutomo Nakai, William B. Isaacs, and William G. Nelson. "Inflammation in Prostate Carcinogenesis." *Nature Reviews Cancer* 7, no. 4 (2007): 256–69. https://doi.org/10.1038/nrc2090.

Dhanasekaran, Saravana M., Terrence R. Barrette, Debashis Ghosh, Rajal Shah, Sooryanarayana Varambally, Kotoku Kurachi, Kenneth J. Pienta, Mark A. Rubin, and Arul M. Chinnaiyan. "Delineation of Prognostic Biomarkers in Prostate Cancer." *Nature* 412, no. 6849 (2001): 822–26. https://doi.org/10.1038/35090585.

Genetics, Myriad. "2019 Prostate Cancer Statistics." Prolaris, April 17, 2019. https://prolaris.com/2019/04/17/2019-prostate-cancer-statistics/.

Horton, Corrigan, Yueli Liu, Chuan Yu, Qing Xie, and Zhu A. Wang. "Luminal-Contact-Inhibition of Epithelial Basal Stem Cell Multipotency in Prostate Organogenesis and Homeostasis." *Biology Open* 8, no. 10 (2019). https://doi.org/10.1242/bio.045724.

Karakiewicz, Pierre, and Sebastiano Nazzani. "A Valuable Tool for Prediction of Repeat Biopsy Pathology." *Nature Reviews Urology* 15, no. 3 (2017): 140–41. https://doi.org/10.1038/nrurol.2017.216.

Koo, Kevin M., Paul N. Mainwaring, Scott A. Tomlins, and Matt Trau. "Merging New-Age Biomarkers and Nanodiagnostics for Precision Prostate Cancer Management." *Nature Reviews Urology* 16, no. 5 (August 2019): 302–17. https://doi.org/10.1038/s41585-019-0178-2.

Kovács, Tünde, Edit Mikó, Gyula Ujlaki, Zsanett Sári, and Péter Bai. "The Microbiome as a Component of the Tumor Microenvironment." *Advances in Experimental* M*edicine and Biology Tumor Microenvironment*, 2020, 137–53. https://doi.org/10.1007/978-3-030-35727-6_10.

Krušlin, Božo, Monika Ulamec, and Davor Tomas. "Prostate Cancer Stroma: an Important Factor in Cancer Growth and Progression." *Bosnian Journal of Basic Medical Sciences* 15, no. 2 (2015). https://doi.org/10.17305/bjbms.2015.449.

Ku, Sheng-Yu, Martin E. Gleave, and Himisha Beltran. "Towards Precision Oncology in Advanced Prostate Cancer." *Nature Reviews Urology* 16, no. 11 (July 2019): 645–54. https://doi.org/10.1038/s41585-019-0237-8.

Leeuwen, Fijs W. B. Van, Alexander Winter, Henk G. Van Der Poel, Matthias Eiber, Nazareno Suardi, Markus Graefen, Friedhelm Wawroschek, and Tobias Maurer. "Technologies for Image-Guided Surgery for Managing Lymphatic Metastases in Prostate Cancer." *Nature Reviews Urology* 16, no. 3 (2019): 159–71. https://doi.org/10.1038/s41585-018-0140-8.

Lupo, Federico, and Molly A. Ingersoll. "Is Bacterial Prostatitis a Urinary Tract Infection?" *Nature Reviews Urology* 16, no. 4 (2019): 203–4. https://doi.org/10.1038/s41585-019-0150-1.

Manzoor, Muhammed A.p., and Punchapaddy–Devasya Rekha. "Microbiome — the Unforeseen Organ." *Nature Reviews Urology* 14, no. 9 (2017): 521–22. https://doi.org/10.1038/nrurol.2017.97.

Mcneal, John E., Elise A. Redwine, Fuad S. Freiha, and Thomas A. Stamey. "Zonal Distribution of Prostatic Adenocarcinoma." *The American Journal of Surgical Pathology* 12, no. 12 (1988): 897–906. https://doi.org/10.1097/00000478-198812000-00001.

Mcneal, John E. "The Zonal Anatomy of the Prostate." *The Prostate* 2, no. 1 (1981): 35–49. https://doi.org/10.1002/pros.2990020105.

Nelson, William G., Karen S. Sfanos, Angelo M. De Marzo, and Srinivasan Yegnasubramanian. "Prostate Inflammation and Prostate Cancer." *Management of Prostate Cancer*, 2012, 103–15. https://doi.org/10.1007/978-1-60761-259-9_6.

NIHR. “MRI Scan before Biopsy Could Detect More Prostate Cancer.” MRI scan before biopsy could detect more prostate cancer. NIHR Dissemination Centre, March 7, 2017. https://discover.dc.nihr.ac.uk/content/signal-000393/mri-scan-before-biopsy-could-detect-more-prostate-cancer.

Peiffer, Lauren B., Sarah L. Poynton, Sarah E. Ernst, Jessica L. Hicks, Angelo M. Marzo, and Karen S. Sfanos. “Inflammation-Associated Pathologies in a Case of Prostate Schistosomiasis: Implications for a Causal Role in Prostate Carcinogenesis.” *The Prostate* 79, no. 11 (2019): 1316–25. https://doi.org/10.1002/pros.23841.

Porter, Corey M., Eva Shrestha, Lauren B. Peiffer, and Karen S. Sfanos. “The Microbiome in Prostate Inflammation and Prostate Cancer.” *Prostate Cancer and Prostatic Diseases* 21, no. 3 (2018): 345–54. https://doi.org/10.1038/s41391-018-0041-1.

“Prostate Biopsy.” Johns Hopkins Medicine. Accessed March 2, 2020. https://www.hopkinsmedicine.org/health/treatment-tests-and-therapies/prostate-biopsy#:~:text=.

Schauer, Isaiah G., and David R. Rowley. “The Functional Role of Reactive Stroma in Benign Prostatic Hyperplasia.” *Differentiation* 82, no. 4-5 (2011): 200–210. https://doi.org/10.1016/j.diff.2011.05.007.

Shibuya, Tadamasa, Go Takahashi, and Tomoko Kan. “Basal Cell Carcinoma of the Prostate: A Case Report and Review of the Literature.” *Molecular and Clinical Oncology*, 2018. https://doi.org/10.3892/mco.2018.1754.

Shrestha, Eva, James R. White, Shu-Han Yu, Ibrahim Kulac, Onur Ertunc, Angelo M. De Marzo, Srinivasan Yegnasubramanian, Leslie A. Mangold, Alan W. Partin, and Karen S. Sfanos. “Profiling the Urinary Microbiome in Men with Positive versus Negative Biopsies for Prostate Cancer.” *Journal of Urology* 199, no. 1 (2018): 161–71. https://doi.org/10.1016/j.juro.2017.08.001.

Sfanos, Karen S, and Angelo M De Marzo. “Prostate Cancer and Inflammation: the Evidence.” *Histopathology* 60, no. 1 (2011): 199–215. https://doi.org/10.1111/j.1365-2559.2011.04033.x.

Sfanos, K. S., B. A. Wilson, A. M. De Marzo, and W. B. Isaacs. “Acute Inflammatory Proteins Constitute the Organic Matrix of Prostatic Corpora Amylacea and Calculi in Men with Prostate Cancer.” *Proceedings of the National Academy of Sciences* 106, no. 9 (June 2009): 3443–48. https://doi.org/10.1073/pnas.0810473106.

Sfanos, Karen S., Heidi A. Hempel, and Angelo M. De Marzo. “The Role of Inflammation in Prostate Cancer.” *Advances in Experimental Medicine and Biology Inflammation and Cancer*, 2014, 153–81. https://doi.org/10.1007/978-3-0348-0837-8_7.

Sfanos, Karen S., Jurga Sauvageot, Helen L. Fedor, James D. Dick, Angelo M. De Marzo, and William B. Isaacs. “A Molecular Analysis of Prokaryotic and Viral DNA Sequences in Prostate Tissue from Patients with Prostate Cancer Indicates the Presence of Multiple and Diverse Microorganisms.” *The Prostate* 68, no. 3 (2008): 306–20. https://doi.org/10.1002/pros.20680.

Sfanos, Karen S., Srinivasan Yegnasubramanian, William G. Nelson, and Angelo M. De Marzo. “The Inflammatory Microenvironment and Microbiome in Prostate Cancer Development.” *Nature Reviews Urology* 15, no. 1 (2017): 11–24. https://doi.org/10.1038/nrurol.2017.167.

Strand, Douglas W, and Andrew S Goldstein. “The Many Ways to Make a Luminal Cell and a Prostate Cancer Cell.” *Endocrine-Related Cancer* 22, no. 6 (2015). https://doi.org/10.1530/erc-15-0195.

Tomas, D, M Ulamec, T Hudolin, S Bulimbašić, M Belicza, and B Krušlin. “Myofibroblastic Stromal Reaction and Expression of Tenascin-C and Laminin in Prostate Adenocarcinoma.” *Prostate Cancer and Prostatic Diseases* 9, no. 4 (February 2006): 414–19. https://doi.org/10.1038/sj.pcan.4500874.

Toom, Emma E. Van Der, Haley D. Axelrod, Jean J. De La Rosette, Theo M. De Reijke, Kenneth J. Pienta, and Kenneth C. Valkenburg. “Prostate-Specific Markers to Identify Rare Prostate Cancer Cells in Liquid Biopsies.” *Nature Reviews Urology* 16, no. 1 (2018): 7–22. https://doi.org/10.1038/s41585-018-0119-5.

Trabzonlu, Levent, Ibrahim Kulac, Qizhi Zheng, Jessica L. Hicks, Michael C. Haffner, William G. Nelson, Karen S. Sfanos, et al. “Molecular Pathology of High-Grade Prostatic Intraepithelial Neoplasia: Challenges and Opportunities.” *Cold Spring Harbor Perspectives in Medicine* 9, no. 4 (June 2018). https://doi.org/10.1101/cshperspect.a030403.

Wang, Zhu A., Roxanne Toivanen, Sarah K. Bergren, Pierre Chambon, and Michael M. Shen. “Luminal Cells Are Favored as the Cell of Origin for Prostate Cancer.” *Cell Reports* 8, no. 5 (2014): 1339–46. https://doi.org/10.1016/j.celrep.2014.08.002.

Wilt, Timothy J., Tien N. Vo, Lisa Langsetmo, Philipp Dahm, Thomas Wheeler, William J. Aronson, Matthew R. Cooperberg, Brent C. Taylor, and Michael K. Brawer. “Radical Prostatectomy or Observation for Clinically Localized Prostate Cancer: Extended Follow-up of the Prostate Cancer Intervention Versus Observation Trial (PIVOT).” *European Urology*, 2020. https://doi.org/10.1016/j.eururo.2020.02.009.

Zhang, Dingxiao, Shuhong Zhao, Xinyun Li, Jason S Kirk, and Dean G Tang. “Prostate Luminal Progenitor Cells in Development and Cancer.” Trends in cancer. U.S. National Library of Medicine, November 2018. https://www.ncbi.nlm.nih.gov/pmc/articles/PMC6212301/.

VITA

William Guzman Jr. was born in Washington, D.C. He received his Bachelor of Arts in Biological Sciences at the University of Maryland, Baltimore County. At a very young age, he showed great interest in art and was often commended for doodling on his assignments in elementary school. Throughout high school, William had internships at the National Museum of Natural History, the United States Botanic Garden, and the Library of Congress, that gave him the opportunity to communicate biological subject matter to visitors. One day during lunch in his undergraduate studies, William attended a guest lecture presented by a faculty of the Johns Hopkins Medical and Biological Illustration graduate program and stumbled upon the world of medical illustration. Through these experiences, William wanted to bridge the artistic world and scientific world to a pursue a career that would bring him joy and curiosity.

In August 2018, William began the Medical and Biological Illustration graduate program in the Department of Art as Applied to Medicine at Johns Hopkins University School of Medicine. At the 2019 Annual Association of Medical Illustration conference, William received an Award of Excellence in the student category for a 3D editorial cover titled, “Nutty Noggin.” He is scheduled to graduate and receive his Master of Arts degree in May of 2020.

After graduation, William plans to teach biomedical processes as a 3D animator using novel techniques and technologies.